PACIFIC EARTHQUAKE ENGINEERING RESEARCH CENTER

Treatment of Uncertainties in Seismic-Risk Analysis of Transportation Systems

Evangelos Stergiou

and

Anne S. Kiremidjian

Stanford University

PEER 2008/02
JULY 2008

Treatment of Uncertainties in Seismic-Risk Analysis of Transportation Systems

Evangelos Stergiou

and

Anne S. Kiremidjian

Department of Civil and Environmental Engineering
Stanford University

PEER Report 2008/02
Pacific Earthquake Engineering Research Center
College of Engineering
University of California, Berkeley

July 2008

ABSTRACT

The objective of this study is to evaluate the consequences of earthquake events to transportation network systems and to develop a probabilistic framework in which to quantify them. The estimation of structural damage to bridges due to earthquakes is discussed, and a methodology is presented to assess the probability density function of the structural loss for single or multiple bridges. The two new uncertainties that are included in the formulations are those related to the replacement cost and the damage factor. Operational loss is computed based on the fixed-demand assumption. The total daily delays of the commuter traffic of the transportation network are used to measure its post-earthquake performance.

The expected value of the annual loss of the transportation network is found to be $13.3M. The operational loss is smaller than the structural loss at low-magnitude ground motions; however, it governs in the higher ground motions. Moreover, the Hayward fault is found to cause higher operational losses than the San Andreas fault. In the evaluation of the probability density function of the structural loss, consideration of the uncertainty in the replacement cost increases the risk. This is not the case when the uncertainty in the damage factor is considered.

ACKNOWLEDGMENTS

This work was supported partially by the Earthquake Engineering Research Centers Program of the National Science Foundation, under award number EEC-9701568 through the Pacific Earthquake Engineering Research Center (PEER). Any opinions, findings, and conclusions or recommendations expressed in this material are those of the author(s) and do not necessarily reflect those of the National Science Foundation.

The partial financial support of the UPS Foundation Endowment provided by Stanford University is also gratefully acknowledged.

The authors would like to thank Caliper Corporation for providing the network analysis software TRANSCAD, which was modified for application to the risk assessment of networks.

CONTENTS

LIST OF FIGURES

LIST OF TABLES

1 Introduction

1.1 MOTIVATION

The 1989 Loma Prieta earthquake closed 142 roads in the San Francisco Bay Area, several of which remained closed for more than six months. Five years later, the 1994 Northridge earthquake produced approximately the same number of closures, with 140 reported. More than a dozen remained closed for months after that event as well. If the San Francisco peninsula segment of the San Andreas fault ruptures, an estimated 428 roads may be put out of commission (ABAG 1997), more than three times the number disrupted by Loma Prieta or Northridge. If the northern segment of the Hayward fault ruptures, nearly 900 roadways could face closure, more than six times the impact from the 1989 event. The worst-case scenario, a rupture along the entire length of the Hayward fault, would close nearly 1500 streets and highways (ABAG 1997).

As societies progress, our activities get more complicated and our time becomes more valuable. Under this perspective, the functionality of transportation networks becomes critical. Until recently, people focused on the direct consequences of earthquakes, such as structural damage or ground failures, but experience has shown that we also need to account for the indirect consequences, and to quantify all the changes that earthquakes cause to our daily activities, personal or professional.

The problem of risk assessment of transportation network systems is relatively new and has been addressed by only a few studies. The problem can be described as a spatially distributed system subjected to various ground excitations due to the same earthquake event. The most vulnerable parts of a transportation system are its bridges; therefore, site-specific analysis is needed to estimate their damage and use it to define its impact on the performance of the network.

1.2 RELATED RESEARCH

Limited studies have investigated the loss of transportation networks due to reduced efficiency. Basoz and Kiremidjian (1996) made the first attempt to quantify for emergency planning purposes the risk to transportation network after an earthquake. Shinozuka et al. (2000) looked at the performance of the highway network in the Los Angeles area after the 1994 Northridge earthquake and developed a probabilistic framework to predict the effect of bridge repairs after the event. In another study for the same area, Shinozuka et al. (2003) used Monte Carlo simulation to estimate the damage of bridges and its consequences to the performance of the transportation network.

Kiremidjian et al. (2003) assessed the damage to the Bay Area transportation network bridges after four earthquake scenarios and estimated the network delays for fixed- and variable post-event trip demand. The same study addresses the problem of post-event emergency response planning and presents a small application for six hospitals located in the East Bay.

Moore et al. (2005) explored the economic impact of electric power loss in the Los Angeles–Orange County area on the transportation network and the local economy. Cho, Fan, and Moore (2003) studied the transportation network variable-demand post-event performance and estimated the losses based on the total delays.

The Federal Emergency Management Agency developed Hazards U.S. (HAZUS), a software for risk mitigation and planning. The methodologies in HAZUS (1999) estimated the structural and downtime losses after natural disasters; however, these methodologies do not have capabilities for transportation network post-event analysis.

Until recently, no software packages were available for the risk assessment of network systems. Absence of software packages means that researchers and practitioners need to develop their own models and assumptions. Further, it is not easy to create benchmarks and compare the results of any analyses. In an effort to overcome this lack of tools, the California Department of Transportation is developing software for Risks from Earthquake Damage to Roadway Systems (REDARS). REDARS is a seismic-risk-analysis software package that estimates the structural and operational losses of transportation network systems, and is expected to enable the California Department of Transportation (Caltrans) to improve its ability to plan for and respond to earthquake emergencies.

1.3 OBJECTIVES AND SCOPE

The goal of this study is to formulate a methodology to quantify the risk to transportation network systems. In contrast to the general norm that deals solely with the estimation of the structural loss, this study proposes a framework that accounts for the operational loss from damage due to network disruption.

Additionally, we will investigate analytically more accurate methods for the estimation of structural loss. Expected value does not seem to be enough for strategic decision making and planning and thus we have to seek more advanced methodologies to account for the uncertainties that are currently ignored.

1.4 ORGANIZATION OF REPORT

Chapter 2 presents the general methodology for the risk analysis of transportation networks. It starts with the structural loss estimation of the bridges of the network and continues with the methodology to obtain the losses due to reduced network efficiency. Finally, it describes the development of the transportation network risk curve.

Chapter 3 consists of two applications. The first is the estimation of the structural and operational loss for the San Francisco Bay Area transportation network for various scenario earthquakes and the development of the annual risk curve. The second application is a demonstration of the framework proposed for the estimation of the probability density function of the structural loss.

Chapter 4 discusses our observations during the elaboration of this study and illustrates our conclusions. Our ideas for future research are also included in the same chapter. The Appendix presents detailed information regarding the HAZUS (1999) methodology for the estimation of the structural loss and explains our assumptions. Tables with the characteristics of all the scenarios investigated are also included in the Appendix.

2 Methodology for Seismic-Risk Assessment

2.1 PROBLEM DEFINITION

The performance of transportation networks when subjected to earthquakes is highly dependent on the performance of their components. These components are subject to various ground motions over time and are expected to experience various levels of damage. Damage at the component level directly affects the functionality of the network. This report assesses the seismic risk not only due to structural loss but also due to post-event network disruption, and express these losses in monetary units.

For the purposes of discussion, the problem is broken into three parts. The first part consists of the risk analysis at the component level (bridges) and the estimation of the structural damage. In the second part we compute the impact of component damage on network functionality. In the last part, we aggregate the losses due to structural damage and network disruption in order to define the total loss.

2.2 NETWORK COMPONENTS RISK ANALYSIS

Estimation of the risk due to structural damage for a specific time window has always been a major challenge for civil engineers. Many probabilistic methodologies have been developed to solve this problem. We use the methodology proposed by the Pacific Earthquake Engineering Research (PEER) Center.

2.3 PEER METHODOLOGY

The PEER methodology is characterized by four generalized random variables: intensity measure (*IM)*, engineering demand parameter (*EDP*), damage measure (*DM*), and decision variable (*DV*). Recognizing the inherent uncertainties involved, these variables are expressed in a probabilistic sense as conditional probabilities of exceedance, i.e., p[A|B]. The PEER equation is shown in Equation 2.1 below.

$$P[DV > dv] = \int\int\int\int dF_{DV|DM} dF_{DM|EDP} dF_{EDP|IM} dF_{IM} \tag{2.1}$$

where

DV	is the decision variable;
DM	is the damage measure;
EDP	is the engineering demand parameter;
IM	is the intensity measure; and
F	is the cumulative distribution of the random variable.

IM represents the hazard uncertainty and is adjusted for the area of interest. It can be either a single variable or a vector of variables. *IM*s are obtained through conventional probabilistic seismic hazard analysis. The most commonly used *IM*s are the peak ground acceleration and the spectral acceleration. Typically, the *IM* is described as a mean annual probability of exceedance, which is specific to the location and design characteristics of the facility. The design characteristics might be described by the fundamental period of vibration, foundation type, material type and geometric parameters.

Given the *IM*, the next step is to perform structural simulations to compute engineering demand parameters (*EDP*), which characterize the response in terms of deformations, accelerations, induced forces, or other appropriate quantities. For buildings, the most common *EDP*s are interstory drift ratios, inelastic component deformations and strains, and floor acceleration spectra. The relationships between *EDP* and *IM* are typically obtained through inelastic simulations, implementing structural, geotechnical, and nonstructural damage simulation models. Various approaches have been considered by the PEER researchers, such as the incremental dynamic analysis technique, to systematize procedures for characterizing the conditional probability, *p[EDP=edp|IM]*, which can then be integrated with the annual probability of exceedance, to calculate mean annual probabilities of exceeding the *EDP*s.

The next step in the process is to perform a damage analysis that relates the *EDP*s to damage measures, *DM*, which describe the physical damage and resulting consequences to a facility that can then be related to the decision variables, *DV*. The *DM*s include descriptions of damage to structural elements, nonstructural elements, and contents, in order to quantify the necessary repairs along with functional or life-safety implications of the damage (e.g., falling hazards, release of hazardous substances, etc.). In our case, where we are dealing with bridges, *DM* describes only the damage to their structural elements. The conditional probability relationships derived, *p[DM=dm|EDP]*, can then be integrated with the *EDP* probability, to give the mean annual probability of exceedance for the *DM*.

The final step in the assessment is to calculate the decision variables, *DV*, in terms of mean annual probabilities of exceedance, *v(DV)*. Generally speaking, the *DV*s relate to one of the three decision metrics that follow, direct dollar losses, downtime (or restoration time), and casualties. In a similar manner as done for the other variables, the *DV*s are determined by integrating the conditional probabilities of *DV* given *DM*, *p[DV=dv|DM]*, with the mean annual *DM* probability of exceedance, *v[DM]*.

2.4 TRANSPORTATION NETWORK RISK ASSESSMENT

Damage to the components of the network often results in the closure of specific links until these components are repaired. This action increases the level of congestion and the travel time. Research has shown (Shinozuka et al. 2003) that these cause a reduction in trip making. This reduction is very difficult to predict; however, logical estimates can be made given the socioeconomic profile of the area of study.

The increase in travel time can be found with respect to the baseline scenario. Of course, the estimation of the delays is strongly correlated to the number of trips that are lost. The problem of the risk assessment of a transportation network becomes more complex under this approach, since the indirect loss has two components that are strongly correlated: the cost of delays and the cost of lost trips.

2.4.1 Traffic Assignment Model

It is impossible to predict human behavior and describe it with a single model. The general accepted principle is that users behave rationally and follow the route perceived as optimum. Several traffic assignment models are characterized by different assumptions. The most popular models are the fixed- and variable-demand models. The formulation of those two models was developed by Moore and Fan (2003) and is summarized in the Highway Demonstration Project (Kiremidjian et al. 2003). We present a brief synopsis of this method for completeness and clarity of the methodology.

The fixed-demand model for traffic assignment assumes that the demand between each origin and each destination is constant and does not change after earthquake events. The advantage of this model is its simplicity. The disadvantage is that it fails when the demand greatly exceeds the capacity of the network due to unrealistic results. The increase of the travel time versus the trips for the fixed-demand model can be seen in Figure 2.1 below.

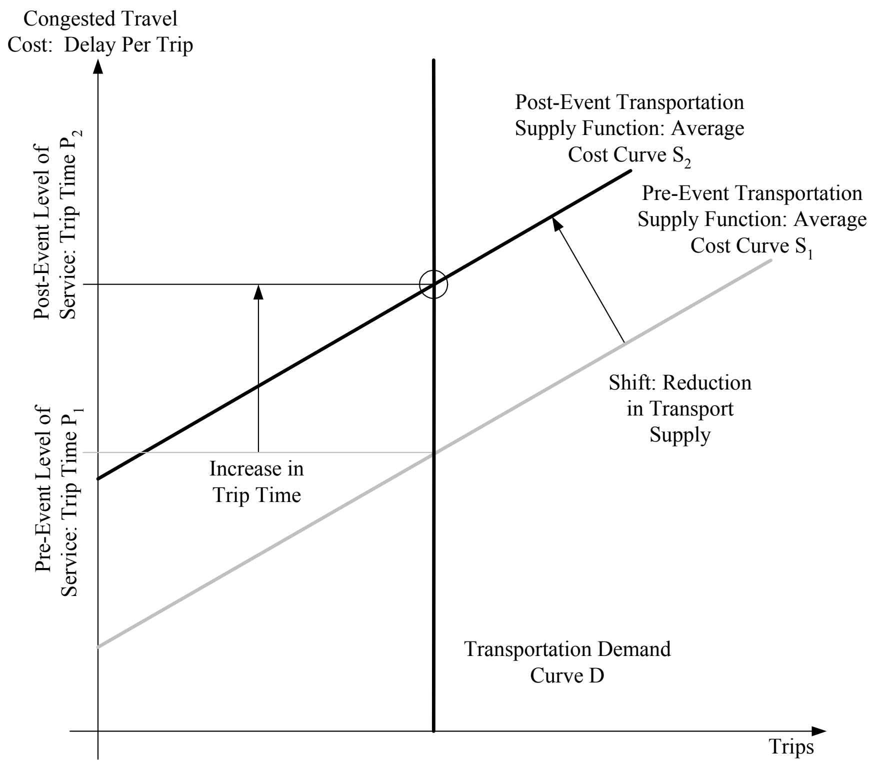

Fig. 2.1 User-equilibrium flows for fixed travel demand (from Kiremidjian at al. 2003, PEER Center Highway Demonstration Project).

As can be seen in Figure 2.1 above, the demand curve is a vertical line and does not change for the different levels of delay. The supply curve is expected to shift upwards after the event, since several links will be shut down. Travel time is the only measure of the network serviceability in this case, since no trips are lost.

The variable-demand model for the traffic assignment assumes that the trip rates are influenced by the level of service of the network. If traveling becomes too expensive in terms of time or distance, the users are expected to change their habits in order to avoid the discomfort. Naturally, this will be the case after a major earthquake event. People will have to accept the new congestion level and decide if they still want to travel or not. It is not easy to define how many passengers will not travel; yet, reasonable assumptions can be made for the function for the trip rate between an origin and a destination and travel time.

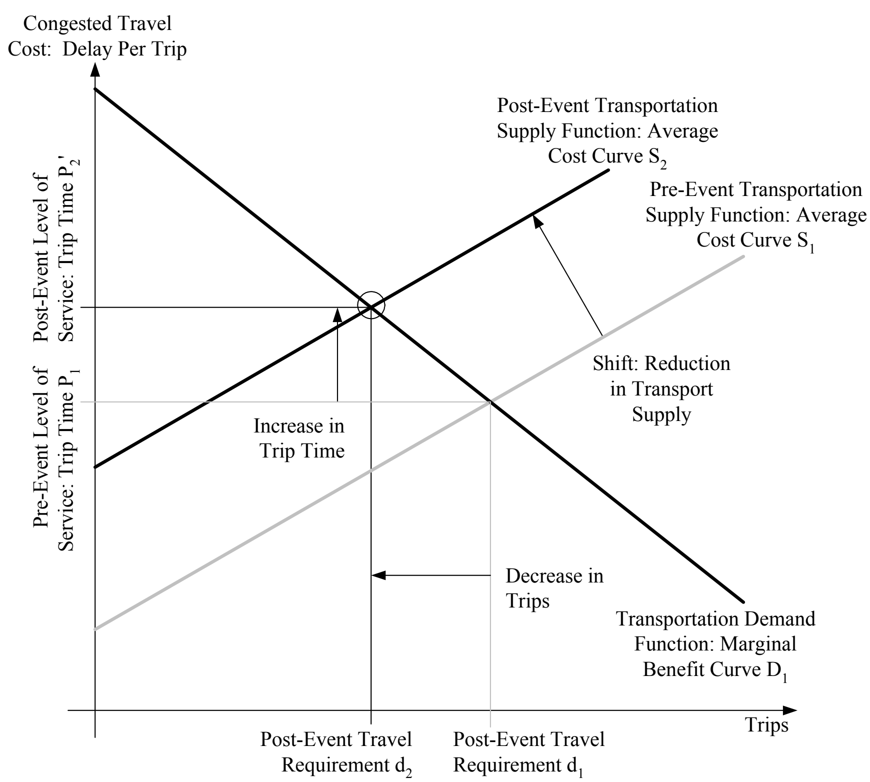

Fig. 2.2 User-equilibrium flows for variable travel demand (from Kiremidjian at al. 2003, PEER Center Highway Demonstration Project).

Figure 2.2 demonstrates the variable-demand model and shows the equilibrium points before and after the event. Prior to the event, the supply of trips in the network is S_1, and P_1 travel time is required for d_1 trips. After the earthquake, the network supply drops to S_2 and the demand responds to this change in performance by dropping at d_2. The travel time at the new equilibrium point is then P_2. It should be noted that the travel time at the equilibrium point for the variable-demand model is less than the corresponding travel time for the fixed-demand model. The loss in this case is due to the travel time increase and due to the cost of the trips forgone.

2.4.2 Traffic Assignment Algorithm

The idea behind the solution of the traffic assignment problem is based on Wadrop's first principle. This principle states that in equilibrium, the journey times in all routes actually used are equal or less than those which would be experienced by a single vehicle on any unused route. Each user noncooperatively seeks to minimize his cost of transportation. The traffic flows that satisfy this principle are usually referred to as "user-equilibrium" (UE) flows, since each user chooses the route that is the best. Specifically, a user-optimized equilibrium is reached when no user may lower his transportation cost through unilateral action.

Wadrop presented the user-equilibrium principle in 1952 and only 4 years later Beckman et al. (1956) compared the equilibrium assignment problem to equilibria problems encountered in theoretical mechanics. One characteristic of such problems is that they may be expressed as extremum problems. He showed that by assuming the cost, c_a, on any link a is a function of the flow x_a, on link a only and that the link performance functions are increasing. Then the flows satisfying Wadrop's first principle are unique and equal to those that minimize Equation 2.2 below.

$$min\, z(x) = \sum_a \int_0^{x_a} c_a(u)\,du \tag{2.2}$$

The method normally used to solve this problem is the convex combination algorithm, originally suggested by Frank and Wolfe (1956) as a procedure for solving quadratic programming problems with linear constraints.

The travel time, c_a, can include numerous components reflecting travel time, number of stops, safety, fuel consumption, etc. Of course, many, if not all, of these components can be expressed as a function of travel time. Therefore, for the purposes of this work, we will use travel time instead of travel cost.

2.4.3 Estimation of Total Loss

The total loss is the summation of the loss due to structural damage and the loss due to network disruption for all the components of the transportation network. The general equation that accounts for the expected value of the two losses is shown below:

$$E(L \mid E) = \int l_s f_{L_s|E}(l_s \mid E)\,dl_s + \int l_n f_{L_n|E}(l_n \mid E)\,dl_n \tag{2.3}$$

where

Ls	is the structural loss of the components;
E	is the scenario event;
L_n	is the loss due to network disruption;
f	is the probability density function of the random variable; and
E(L|E	is the expected value of L given E.

The structural loss described in Equation 2.3 can be estimated based on the PEER methodology described above. The operational loss in the same equation requires traffic assignment software. This software must allocate the traffic within the components of the network based on the supply and the demand for trips. The results of such an analysis are the flow and the time needed to travel through each component.

The annualized risk for the system from all possible events that occur with rate v_i is expressed in Equation 2.4 below. It uses the results of Equation 2.3 or a sample scenario and then finds the results for all possible scenarios.

$$E(L \mid E) = \sum_{all\ events} v_i * \left\{ \int l_s f_{L_s|E}(l_s \mid E)\,dl_s + \int l_n f_{L_n|E}(l_n \mid E)\,dl_n \right\} \tag{2.4}$$

where

L_s is the structural loss of the components;

E is the scenario event;

L_n is the loss due to network disruption;

f is the probability density function of the random variable; and

v is the rate of occurrence of the event in the forecast period.

2.5 GENERAL APPROACH

The probabilistic framework for risk analysis of network systems is presented in this section. It is characterized by three parts. The first part of the framework deals with the hazard analysis and the second with the assessment of the structural loss. Network analysis is the last part and is based on the results of the previous analyses.

2.5.1 Seismic Hazard Analysis

Seismic hazard analysis is the study of expected earthquake ground motions at any point on the earth. In the PEER framework, seismic hazard analysis is used to define the *IM* level at the site of interest. There are several descriptors that can be used to quantify the *IM*. These include peak ground acceleration, spectral acceleration, peak ground displacement, moment magnitude and distance. The use of vectors with combinations of *IM*s is also an option. In this study, the spectral acceleration at the first mode of vibration of each bridge (S_a) and the peak ground deformation (PGD) are used to define the bridge damage.

The choice of *IM*s is consistent with the HAZUS (1999) methodology we use for the structural loss estimation. This methodology relates the structural damage with the PGD and S_a at the site. Particularly, the spectral acceleration is used for the estimation of the ground shaking damage and the peak ground deformation for the estimation of the ground failure damage.

2.5.1.1 Estimation of Spectral Acceleration

There are many attenuation functions available for our area of study that are updated periodically. We use the Boore, Joyner, and Fumal (1997) attenuation function. This function estimates the horizontal response spectra and peak acceleration for shallow earthquakes in western North America. It gives ground motion in terms of spectral acceleration at the predominant period of the structure and is a function of moment magnitude, distance, and site conditions for strike-slip, reverse-slip, or unspecified mechanisms. The general equation of the attenuation function follows:

$$\begin{gathered}
\ln Y = b_1 + b_2 * (M-6) + b_3 * (M-6)^2 + b_5 * \ln r + b_v * \ln\left(\frac{V_s}{V_A}\right) \\
\text{where } r = \sqrt{r_{jb}^2 + h^2} \\
\text{and } b_1 = \begin{cases} b_{1SS} & \text{for strike slip earthquakes} \\ b_{1RS} & \text{for reverse slip earthquakes} \\ b_{1All} & \text{if mechanism is not specified} \end{cases}
\end{gathered} \tag{2.5}$$

In the previous equation, Y is the ground motion parameter such as PGA or S_a in terms of g. The predictor variables are moment magnitude (M), distance (r_{jb} in km), and average shear wave velocity (V_s, in m/sec). Coefficients to be determined are b_{1SS}, b_{1RS}, b_{1All}, b_2, b_3, b_5, b, and V_A. They are given by Boore, Joyner, and Fumal. The distance r_{jb} is equal to the closest distance from the site to a point on earth's surface that lies directly above the fault rupture. The parameter h is a fictitious depth that is determined by regression and is also given by the authors.

The shear wave velocities used are those suggested by the National Earthquake Hazards Reduction Program (NEHRP 1997). For the intermediate soil classes, we assume that the shear wave velocity is the average of the shear wave velocities of the adjacent soil classes. The average shear wave velocities for each soil class are presented in Table 2.1.

Table 2.1 NEHRP shear wave velocities (1997).

NEHRP Site Class	Average shear velocity (m/sec)
B	1070
C	520
D	250
E	180

2.5.1.2 Estimation of Permanent Ground Deformation

We account for two causes of ground failure: liquefaction and landslide. In case they both occur at a bridge site, we assume that the maximum deformation governs. This assumption yields that:

$$PGD = max\{ PGD_{Liquefaction}, PGD_{Landslide} \} \tag{2.6}$$

where

$PGD_{Liquefaction}$ is the permanent ground deformation due to liquefaction; and

$PGD_{Landslide}$ is the permanent ground deformation due to ground settlement.

2.5.1.3 Liquefaction

Liquefaction is a soil-behavior phenomenon in which excess pore pressure is generated under undrained loading conditions. For saturated cohesionless soils, static and cyclic loading cause rapid loading to occur under undrained conditions. The tendency for densification causes excess pore pressures to increase and effective stresses to decrease. Liquefaction results in permanent ground deformation such as settlement and/or lateral spreading.

The permanent ground deformation is computed at each bridge site due to lateral spreading and ground settlement according to the methodology presented in HAZUS (1999). The maximum of the deformations due to the two different hazards is used for the estimation of the damage due to liquefaction. A detailed description of the methodology followed for the liquefaction analysis is presented in Appendix A.

2.5.1.4 Landslide

Landslide is the rapid slipping of a mass of earth or rock from a higher elevation to a lower level under the influence of gravity and water lubrication. More specifically, rockslides are the rapid downhill movement of large masses of rock with little or no hydraulic flow, similar to an avalanche. Earthquake-induced landsliding occurs when the static plus inertial forces within the slide mass exceed the friction forces of the slide mass. The minimum value of the peak ground acceleration within the slide mass required to cause this failure is denoted by the critical or yield acceleration a_c.

The permanent ground deformation due to landslides is computed at each bridge site according to HAZUS (1999). The complete methodology followed is described in Appendix B for reference.

2.5.2 Generation of Fragility Curves

Fragility curves are conditional cumulative distribution functions that define the exceedance probability of a damage state for a given level of ground shaking or ground deformation. The five damage states considered in this study are None, Slight, Moderate, Extensive, and Complete. The HAZUS (1999) recommendation for the damage states is summarized as follows:

Slight Damage is defined by minor cracking and spalling to the abutment, cracks in shear keys at abutments, minor spalling and cracks at hinges, minor spalling at the column (damage requires no more than cosmetic repair), or minor cracking to the deck.

Moderate Damage is defined by any column experiencing moderate (shear cracks) cracking and spalling (column structurally still sound), moderate movement of the abutment (<2''), extensive cracking and spalling of shear keys, any connection having cracked shear keys or bent bolts, keeper bar failure without unseating, rocker bearing failure or moderate settlement of the approach.

Extensive Damage is defined by any column degrading without collapse—shear failure—(column structurally unsafe, significant residual movement at connections, or major settlement approach, vertical offset of the abutment, differential settlement at connections, shear key failure at abutments.

Complete Damage is defined by any column collapsing and connection losing all bearing support, which may lead to imminent deck collapse or tilting of substructure due to foundation failure.

The probability of being or exceeding a damage level is modeled with a cumulative lognormal distribution. Such a distribution is expressed in Equation 2.7 below.

$$P[DS_s \mid IM] = \Phi\left[\frac{1}{\beta_{ds}}\left(\frac{IM}{S_{median}}\right)\right] \tag{2.7}$$

where

β_{ds} is the standard deviation of the natural logarithm of spectral acceleration of damage state *ds;*

IM is the intensity measure, usually PGA or PGD;

S_{median} is the median value of the of PGA or PGD at which the bridge reaches the threshold of the damage state *ds;* and

Φ is the standard normal cumulative distribution function.

There are three methods for developing fragility functions: heuristic, empirical, and analytical. Heuristic methods are based on learning that takes place through discovery. The Applied Technology Council Technical Report 13 fragility functions fall into this category. Empirical fragility functions are based on data from past earthquakes. The most popular empirical fragility functions are probably the ones suggested by Shinozuka et al. (2000) and Kiremidjian et al. (1999, 2004), using data from the Northridge earthquake. Analytical fragility functions are based on mathematical frameworks and are usually combined with simulations. Such fragility functions were introduced by Basoz and Mander (1999), Mackie and Stojadinovic (2001, 2004), Des Roches (2004), and Shinozuka et al. (2000).

In this study fragility functions are required for all bridge classes found in a region. The fragility functions developed by Mackie and Stojadinovic provide information only for two bridge categories. Fragilities by Des Roches are developed for bridges in the central US and, finally, the functions introduced by Shinozuka use a bridge classification system other than the HAZUS (1999) and thus cannot be adopted. Considering the above constraints, we can only adopt the Basoz and Mander (1999) fragility functions. A detailed description of the methodology proposed by Basoz and Mander (1999), is also included in the HAZUS (1999) technical manual and can be found in Appendix C.

2.5.3 Damage Factor

The scope of fragility functions is to provide the probability of being or exceeding each damage state. Damage state expresses a range of damage. This range is completely subjective and depends on the methodology used. It is characterized by a central damage factor, a minimum and a maximum value. In the HAZUS methodology used in this study, extensive damage state means that the damage varies from 15% to 40% of the replacement cost of the bridge. Table 2.2 describes the bounds considered for each damage state.

Table 2.2 Variation of damage for each damage state (modified by HAZUS).

HAZUS Damage State	Central Damage Factor	Minimum Damage Factor	Maximum Damage Factor
None	0.00	0.00	0.00
Slight	0.03	0.01	0.03
Moderate	0.08	0.03	0.15
Extensive	0.25	0.15	0.40
Complete	1.0 if n <3 2/n if n≥3	0.40	1.00
*n = number of spans			

For the fragility curves shown in Figure 2.3 below, there is a 65% probability of being in the slight damage state or higher, 50% for the moderate damage state or higher, 38% for the extensive damage state or higher, and 19% for the complete damage state or higher when the PGA equals 1.0g. The probability of being in a specific damage state can be computed from the differences of the exceedance probabilities at each ground motion level. If we multiply these probabilities with the central damage factors of each damage state, we obtain the expected value of the damage of the component.

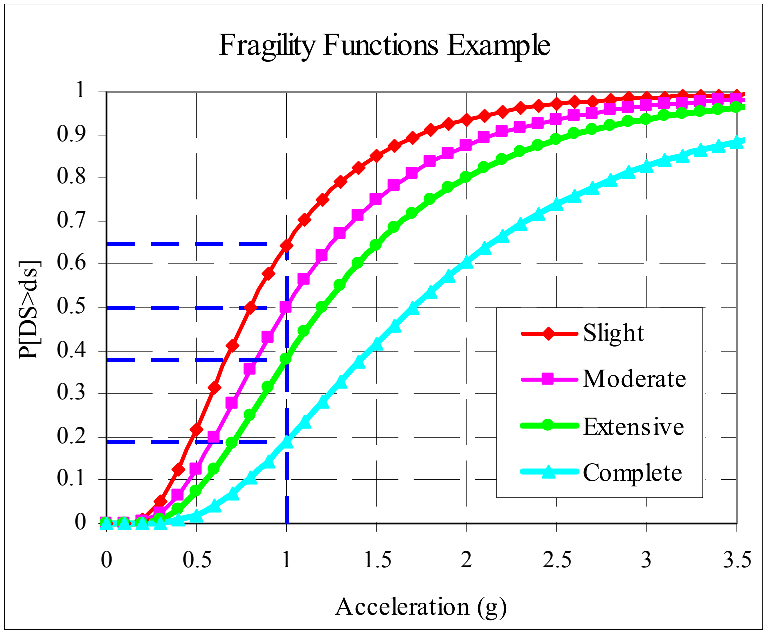

Fig. 2.3 Example fragility functions for single-span highway bridges (HAZUS bridge class 4).

Since we have two possible failure modes, ground shaking and ground failure, we select the maximum damage each time and evaluate the loss based on the damage caused from that hazard.

2.5.4 Evaluation of Structural Loss for a Single Site

Two different methodologies are presented for the estimation of the direct loss. The first is the methodology suggested by HAZUS (1999). It computes the expected value of the loss. The second is an approach by the authors and it evaluates the probability density function of the loss. In both approaches, we deal with ground shaking and ground failure separately and we keep the dominating hazard, since we cannot have two different failure modes occurring at the same time. Namely, we have:

$$Loss = max\langle Loss_{GS}, Loss_{GF} \rangle \tag{2.8}$$

where

$Loss_{GS}$ is the loss due to ground shaking; and

$Loss_{GF}$ is the loss due to ground failure.

2.5.4.1 Estimation of Expected Value of Structural Loss for a Single Site

The computation of the expected value of the loss uses the mean value of the intensity measure as input to the fragility functions. The probability of being at each damage state is then defined separately for ground shaking and ground failure. The product of this probability with its central damage factor gives the expected value of the damage of the bridge for that event. If we know the replacement cost of the bridge we are studying, we can determine that the expected loss is nothing more than the product of the damage factor and the replacement cost of the component.

The replacement cost for a single bridge is computed after the methodology suggested by Caltrans. According to this methodology, the replacement cost of a bridge is the product of its deck area and a constant number, its comparative cost. The comparative bridge cost expresses the cost per area (in $/m^2 or $/ft^2) to rebuild the bridge and depends on its structural characteristics. The comparative bridge costs used in this study are provided by Caltrans (2004).

The advantage of this methodology is that it is easy to apply and requires only keeping track of the mean value of the loss of each bridge. The disadvantage of this approach is that the loss estimates depend on the replacement cost we assign to each component. Furthermore, we do not get information for the skewness or the properties of the loss distribution, making it difficult to allocate resources for retrofit, repair, and replacement of bridges that are consistent with the exposure risks.

$$
\begin{aligned}
E(l) &= RC * max\left\{ \sum_{all\ DS_i}\{CDF_i * P[DS_i \mid PGA]\}, \sum_{all\ DS_i}\{CDF_i * P[DS_i \mid PGD]\} \right\} \\
\sigma_i^2 &= RC^2 * \sum_{all\ DS_i}\{CDF_i^2 * P[DS_i \mid IM]\} - E(l)^2
\end{aligned}
\tag{2.9}
$$

where

l is the loss for one bridge;

RC is the replacement cost of the bridge;

CDF is the central damage factor (Table 2.2);

DS is the damage state;

PGA is the peak ground acceleration; and

σ_i is the variance of the direct loss of one bridge.

2.5.4.2 Estimation of PDF of Structural Loss for a Single Site

Expected value computations provide an estimate of the mean value of the potential loss of a component; however, they cannot provide information regarding the properties of the decision variable and its dispersion. In order to assess the probability density function of the loss, we need to evaluate its conditional density.

Our enhancement of the general PEER equation used in this study makes two new assumptions: (1) the damage factor of each damage state is a truncated normal random variable, bounded between the damage factor limits set by HAZUS (1999) for each damage state and (2) the replacement cost of the structure is a truncated random variable following a normal distribution.

2.5.4.3 Modeling of Damage Factor Uncertainty

By definition, the damage factor is equal to the quotient of the damage (expressed in monetary units) by the replacement cost. It is a damage measure varying from zero to one. According to HAZUS (1999), each damage state expresses a range of damage factors. Each range is not equal to the others. In the expected value computation, where we use a central damage factor for each damage state, this difference in the damage factor variation between the different damage states cannot be taken into account. For instance, in slight damage state, damage varies from 1% to 3% compared to 40% to 100% for the complete damage state. We find that this difference in the damage dispersion between the damage states is important and should be reflected in our computations.

To this effort, we assign a truncated normal distribution to the damage factor. We assume the mean to be equal to the central damage factor and the coefficient of variation to be equal to 30% (or δ=0.30). The truncation of the distribution is done at the minimum and maximum damage factors of the damage state. The distribution follows:

$$f_X(x) = N * \frac{e^{-\frac{(x-\mu)^2}{2\sigma^2}}}{\sigma\sqrt{2\pi}}, \quad a < x < b \tag{2.10}$$

$$\sigma_x = 0.30 * \mu_x \tag{2.10a}$$

$$N = \frac{1}{F_X(b) - F_X(a)} \tag{2.10b}$$

where

μ_X is the central damage factor of the damage state;

σ_X is the standard deviation computed according to 2.10a;

N is the normalization factor defined in 2.10b;

a, b are the truncation bounds each damage state;

$f_X(x)$ is the PDF of the damage factor; and

$F_X(x)$ is the CDF of the damage factor.

The damage factors for each damage state as well as the properties we used for their modeling as random variables are given in Table 2.3. The distributions of damage states are shown in Figure 2.4.

Table 2.3 Properties of damage factor for each damage state.

HAZUS Damage State	Central Damage Factor	Minimum Damage Factor	Maximum Damage Factor	δ	N
None	0.00	0.00	0.00	0.00	-
Slight	0.03	0.01	0.05	0.30	0.974
Moderate	0.08	0.05	0.15	0.30	0.893
Extensive	0.25	0.15	0.40	0.30	0.886
Complete	0.70	0.40	1.00	0.30	0.847

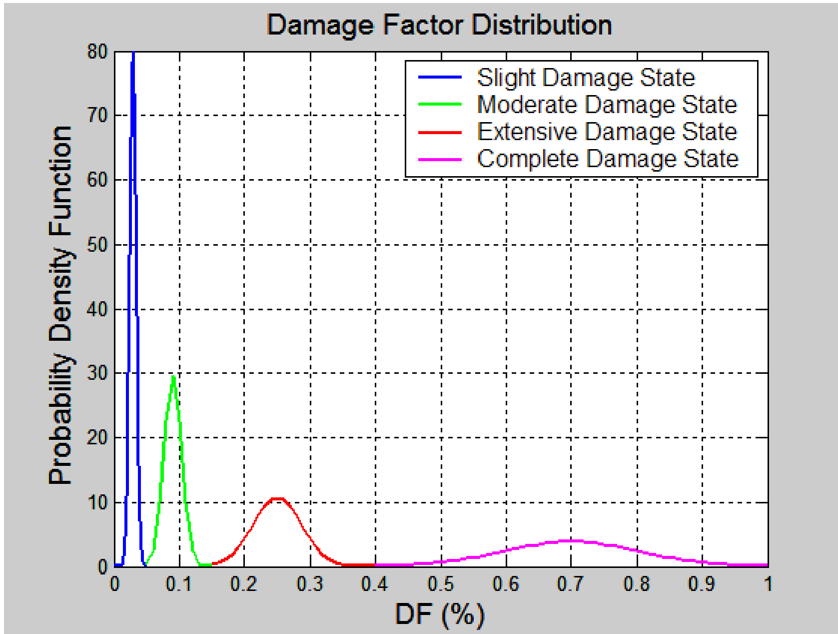

Fig. 2.4 Probability density functions of damage factor.

2.5.4.4 Modeling of Replacement Cost Uncertainty

The replacement cost of a structure is usually estimated by experts or by the owner. It is based on assumptions for the resources we would need today to rebuild the structure. This way, errors in the estimation of the replacement cost will be directly reflected on the loss computations.

The reason we propose variable replacement cost is two-fold. First, we believe it is not easy to predict the future replacement cost of a structure and, second, the current methodologies for this estimation are very abstract, at least for the time being (e.g., area of bridge deck multiplied by a constant).

In our approach, we assume that the replacement cost is a truncated normal random variable with mean value equal to the replacement cost we get through the Caltrans method described earlier. The standard deviation is assumed to be 50% of the mean value (or δ=0.5). The equation for the replacement cost uncertainty follows.

$$f_Y(y) = N * \frac{e^{-\frac{(y-\mu)^2}{2\sigma^2}}}{\sigma\sqrt{2\pi}}, \quad c < y < d \tag{2.11}$$

$$\sigma_y = 0.5 * \mu_y \tag{2.11a}$$

$$N = \frac{1}{F_Y(d) - F_Y(c)} \tag{2.11b}$$

where

- μ_y is the replacement cost we get according to Caltrans;
- σ_y is the standard deviation computed according to 2.11a;
- N is the normalization factor defined in 2.11b;
- c, d are the truncation bounds taken as 50% and 150% of the mean value;
- $f_Y(y)$ is the PDF of the replacement cost; and
- $F_Y(y)$ is the CDF of the replacement cost.

2.5.4.5 Loss PDF Computation

Based on the modeling discussed earlier, we need to modify the general PEER equation for ground shaking and ground failure and account for the new uncertainties that are introduced. In that case the formulas for the damage from ground shaking and ground failure become:

Ground Shaking

$$P[L > l_I] = \int\int\int\int\int dF_{L|RC,\,DF,\,Sa} dF_{RC} dF_{DF|Sa} dF_{DS|Sa} dF_{Sa} \tag{2.12a}$$

Ground Failure

$$P[L > l_I] = \int\int\int\int\int dF_{L|RC,DF,PGD} dF_{RC} dF_{DF|DS} dF_{DS|PGD} dF_{PGD|PGA} dF_{PGA} \tag{2.12b}$$

where

- PGA is the peak ground acceleration;
- PGD is the permanent ground deformation;
- DS is the damage state;
- DF is the damage factor depending on the damage state;
- RC is the replacement cost; and
- L is the structural loss.

The computations of Equations 2.12a and 2.12b cannot be done analytically because of the nature of the distributions involved. Thus, we need to evaluate the integrals numerically. The formula used for the numerical integration follows:

$$P[L > l_l] = \sum_{all\ PGA} \sum_{all\ DS} \sum_{all\ DF} \sum_{all\ RC} \sum_{all\ L>L_l} P_{[L|DF,RC]} P_{[RC]} P_{[DF|DS]} P_{[DS|PGA]} P_{[PGA]} \tag{2.13a}$$

$$P[L > l_l] = \sum_{all\ PGA} \sum_{all\ PGD} \sum_{all\ DS} \sum_{all\ DF} \sum_{all\ RC} \sum_{all\ L>L_l} P_{[L|DF,RC]} P_{[RC]} P_{[DF|DS]} P_{[DS|PGA]} P_{[PGD|PGA]} P_{[PGA]} \tag{2.13b}$$

where

P[X|Y] = P[X=x|Y] for general random variables X and Y.

For each loss level, we can find its probability of exceedance through Equations 2.13a and 2.13b for the ground shaking and the liquefaction hazard, respectively. If we repeat this computation for values of the loss covering the range of the possible values of the repair cost, we generate a curve that is the complementary CDF of the loss for each hazard. We can also differentiate the CDFs to obtain their generating PDFs. As discussed earlier, we keep the loss curve of the hazard that governs, since we cannot have two failure modes at the same time.

2.5.5 Estimation of Expected Value of Structural Loss for Multiple Sites

Decision makers are usually interested in methodologies that are applicable to multiple bridges, in order to make decisions for retrofitting strategies or planning. In this section, we will generalize the two methods for the estimation of the loss at a single site and apply them to a set of bridges.

According to probability theory, the sum of the expected values of the loss of all the components will be equal to the expected value of the total loss. The variance of the total loss is equal to the sum of the variances, under the assumption that the damage of the components is independent. The equations follow:

$$E(Total\ Loss) = \sum_{all\ bridges} \{E(l_i)\}$$
$$\sigma^2 = \sum_{all\ bridges} \sigma_i^2 \tag{2.14}$$

where

$E(l_i)$ is the expected value of the loss at a single site; and

σ_i is the variance of the loss at a single site.

2.5.6 Evaluation of PDF of Loss at Multiple Sites

Equations 2.13a and b provide information for the probability density function of the loss of each component for the different hazards. We need to aggregate all those PDFs and obtain the distribution of their sum. This aggregation can be done through the convolution density formula.

$$L_{total} = L_1 + L_2 + L_3 + \ldots + L_n \tag{2.15}$$

$$f_{L_{total}} = f_{L_1} \otimes f_{L_2} \otimes f_{L_3} \otimes \ldots \otimes f_{L_n} \tag{2.16}$$

where

L_{total} is the total loss for the set of bridges;

L_i is the loss of a single bridge;

f is the PDF of a random variable; and

$\otimes$ is the symbol for convolution.

Using this property, convolution in the time domain becomes multiplication in the frequency domain and can be computed by transforming the individual PDFs of the loss, f_L, into the frequency domain, multiplying them in the same domain, and then doing the inverse transformations to convert the result back to the time domain. In our case, we used successive convolutions of two random variables because, this way, the numerical error is reduced.

2.5.7 Evaluation of Network Loss

Undoubtedly, the network performance drops after an earthquake event because of the decrease of the capacity or the closure of its components. The question is how much. The methodology followed in this study estimates the operational loss of the network relative to the baseline performance, which is the performance prior the earthquake.

The damage of each of the components of the network computed above is used to reduce the capacity. For example, a bridge with 20% damage will have to reduce its traffic by the same percentage in order to reduce the acting loads. When the damage exceeds 40%, we assume that the bridge is closed and passengers have to detour.

The total travel time for the modified network is estimated and its difference with the baseline scenario travel time is found. It is possible to convert this delay to monetary units, if we know the value of time and the number of passengers.

As time passes, some bridges are repaired and become functional again. In order to have a realistic assessment of the total operational loss, we have to account for its evolution over time. To this effort, we are using the HAZUS estimates for the downtime for the different damage states and perform network analyses immediately after the event and after 1, 3, 7, 14, 30, 180 and 365 days. This way, we create a curve with the change of the operational loss over time. The total indirect loss is the integral of this curve and must be added to the structural loss in order to estimate the total loss of the scenario. The time to restoration for each damage state is taken after HAZUS (1999) and is shown in Table 2.4 below.

Table 2.4 Repair time (from HAZUS 1999).

Damage State	Highway Bridges Mean (days)
Slight/Minor	0.6
Moderate	2.5
Extensive	75.0
Complete	230.0

2.5.8 Uncertainties in Loss Estimation

The term uncertainty in statistics means a risk that has not been measured. It reflects the amount that an observable quantity may differ from its real value. In general, there are two kinds of uncertainties, epistemic and aleatoric.

Aleatoric uncertainty is randomness which is usually modeled by probability distributions. Epistemic uncertainty is a knowledge gap: our understanding of the phenomena is incomplete or erroneous, so models of the phenomena are uncertain. Often the random (aleatoric) elements of the phenomena are poorly understood, so probability models are themselves subject to epistemic uncertainty as well.

2.5.8.1 Uncertainties in Direct Loss Estimation

The methodology used in this study for the computation of the direct loss involves several uncertainties. In particular, the *IM* distribution is accompanied by the aleatoric uncertainty of the ground motion given the characteristics of the earthquake and the extent of the fault rupture given the location and the magnitude. Moreover, the ground motion attenuation model used (Boore, Joyner, and Fumal 1999) and the geometric characteristics of the fault also include epistemic uncertainty.

Fragility functions include epistemic uncertainty in the assumptions needed for the structural and geometric characteristics of the structure as well as for the models to develop them. They also ignore the three-dimensional effects in the response of the structure and its interaction with the soil.

Damage states have epistemic uncertainties associated with the establishment of the structural response and the assessment of the damage factor. Finally, our estimates for the replacement cost of the structures are based on expert opinion and on future predictions for labor cost, cost of materials, etc. The last two assumptions also introduce epistemic uncertainty.

2.5.8.2 Uncertainties in Operational Loss Estimation

The transportation network operational loss evaluation is based on the estimation of the structural loss; therefore, all the uncertainties associated with it are expected to propagate in the operational loss computations.

The damage of each of the components given an earthquake event is not known with certainty and the user-equilibrium algorithm for the traffic assignment cannot model it as a random variable. Only stochastic network analysis can solve the network problem with time-varying link travel times, yet such an analysis would go beyond the goals of this study. Also, because of the size of the area of interest, any probabilistic approach of the network becomes too expensive in terms of computational running time. Dynamic and nondynamic stochastic networks are presented in the paper by He, Kornhauzer, and Ran (2002), and future research should investigate their application to seismic-risk assessment of transportation networks.

The user-equilibrium algorithm for the traffic assignment is also based on assumptions about the behavior of passengers, which is random in reality. In addition, our assumption regarding the demand and the supply of trips in the network is associated with epistemic uncertainty. Another source of uncertainty in the operational loss computation is associated with the assumptions made about socioeconomic factors, like the value of the time or the passenger-car occupancy.

2.6 TRANSPORTATION NETWORK RISK CURVE DEVELOPMENT

Scenario-based analysis is useful and can reveal the weaknesses of the transportation network system being investigated; however, it does not provide information about the likelihood of the scenarios we are studying.

The alternative to this deterministic approach is the probabilistic approach in order to develop a risk curve for the total loss of the network. This curve will express the structural and the operational loss of the network in a probabilistic context. That is considering all the possible scenarios and estimating the probability of exceeding each loss level.

In general, there are three methods to develop a risk curve: (1) analytical methods, (2) Monte Carlo simulations, and (3) importance sampling. Analytical methods consider the full assessment of the equations describing the risk model. Monte Carlo simulation is an approximate method that randomly selects scenarios over time and evaluates the loss. It has to be repeated many times to obtain stable results or it needs to be run over long forecast periods to capture all possible events. Importance sampling is again a simulation-based approach that selects scenarios in the region where the function being integrated (loss) is large.

Considering the nature of the transportation network problem, we cannot use analytical methods for the risk assessment. Of the two remaining applicable methods, we choose to follow the importance sampling method because it minimizes the analyses that have to be performed without loss in accuracy.

We investigate the San Andreas and the Hayward faults and account for all the scenarios that exceed moment magnitude 6.75. The probability of each scenario occurring within a certain time horizon is defined with Equation 2.17, and the total loss (structural and operational) is computed. We then rank the losses and find the probability of exceeding each of them according to Equation 2.18:

$$P[E_i] = v_{m_o} * P[m_i = M \mid m_i > m_o] * P[location \mid m_i] \tag{2.17}$$

where

v_{mo}	is the rate of exceeding m_o within the time horizon investigated. In our case, the forecast period is one year;
$P[m_i=M \mid m_i > m_o]$	is the probability of experiencing a specific moment magnitude;
$P[location \mid m_i]$	is the probability of the location of the rupture; and
$P[E_i]$	is the probability of event E_i occurring.

$$L_n > L_{n-1} > ... > L_k > ... > L_1 \;\; then \;\; P[L_k \geq l] = 1 - \prod_{i=k}^{n} \left(1 - P[E_i]\right) \tag{2.18}$$

where

L_n	is the total loss after event n;
$P[E_i]$	is the probability of event E_i occurring; and
$P[l>L_k]$	is the probability of exceeding L_k.

It should be noted that the probability of experiencing a certain magnitude is computed based on the magnitude density function shown in Equation 2.19.

$$f_M(m) = \frac{\beta e^{-\beta(m-M_L)}}{1-e^{-\beta(M_U-M_L)}} \;,\; for\ M_L \leq m \leq M_U \;\; and \;\; \beta > 0 \tag{2.19}$$

where

M_U, M_L	are the minimum and the maximum events considered; and
β	is a parameter computed by regression analysis of the historical data of the fault.

All the fault segments are assumed to be equally likely to rupture; therefore, the probability of the location depends only on the number of the scenarios we are investigating. For example, consider an event in a fault with total length equal to 120 km and rupture length equal to 30 km. Assume we want to examine 10 scenarios. In that case, each of the scenarios will be assigned 10% probability and we will slide the rupture 10 km each time. In this way we will have 10 different positions for the rupture locations.

3 Application to San Francisco Bay Area Transportation Network

3.1 DATA SYNTHESIS

A demonstration of the methodologies explained in the previous chapter is presented here in. We study the San Francisco Bay Area transportation network and its components and we predict the total loss not only due to structural damage but also due to network disruption. For the loss due to network disruption, we compute it until the network is fully repaired. Based on our loss estimates from the scenario events and their corresponding annual rate of occurrence, we develop the annual risk curve of the Bay Area transportation network due to the hazards of the San Andreas and the Hayward faults. In the last section, we demonstrate the computation of the distribution of the loss for a portfolio of ten bridges and its sensitivity to the uncertainties we introduce.

3.2 CLASSIFICATION OF BRIDGES

The bridge database used in this study contains 2921 state and local bridges in five counties of the San Francisco Bay Area. The database with bridge locations and physical characteristics is provided by the California Department of Transportation (Caltrans). Of all the bridges, 281 are excluded from the analyses for various reasons (e.g., pedestrian and railroad bridges, and bridges lacking sufficient information) and 1515 cannot be included in our transportation network model, either because they belong to the street network or because we do not have sufficient information to assign them to the appropriate link. Figure 3.1 below gives the spatial distribution of the 1125 bridges used in the study and Table 3.1 shows their categorization by type and by county.

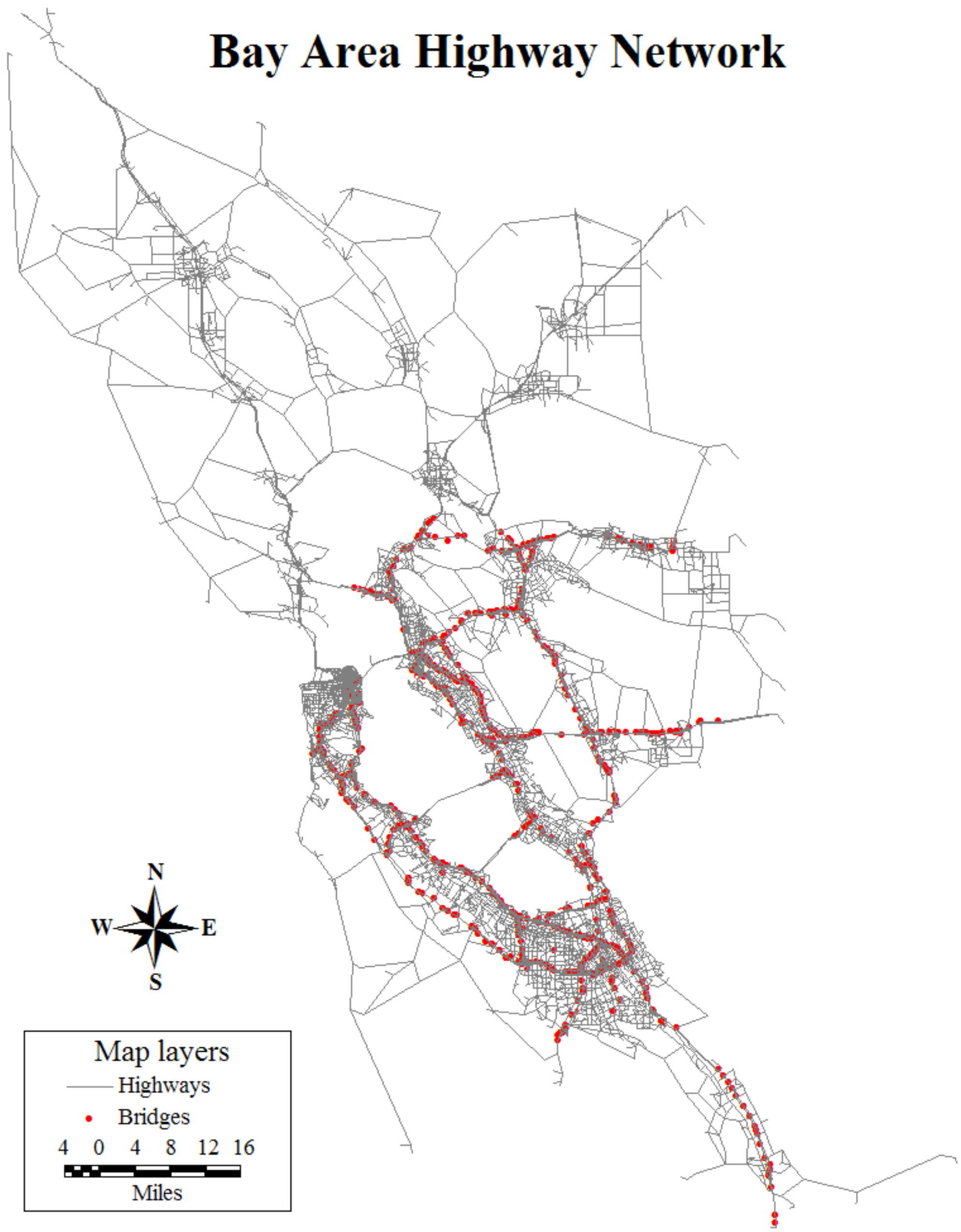

Fig. 3.1 Bay Area highway network.

All the bridges are classified into 28 classes based on their structural properties according to the HAZUS (1999) technical manual. The last bridge class (28th) includes all bridges that have unknown characteristics. This classification brings into the same class many bridges which have nothing in common, yet they are treated as if they are similar.

Table 3.1 Bridges by county and type.

County	State Bridges	Local Bridges	Total Number of Bridges	Number of Bridges Used
Alameda	505	243	748	360
Contra Costa	291	320	611	208
San Francisco	104	53	157	63
San Mateo	234	140	374	164
Santa Clara	552	479	1031	330
Total	1686	1235	2921	1125

The local soil conditions are provided by the California Geological Survey (CGS) while the liquefaction susceptibility categories are obtained from the US Geological Survey Open File Report 00-444 (USGS 2000). Figure 3.2 below shows the local soil conditions in the study area according to the eight National Earthquakes Hazards Reduction Program (NEHRP 2000) site categories, ranging from firm soil (class B) to bay mud (class E).

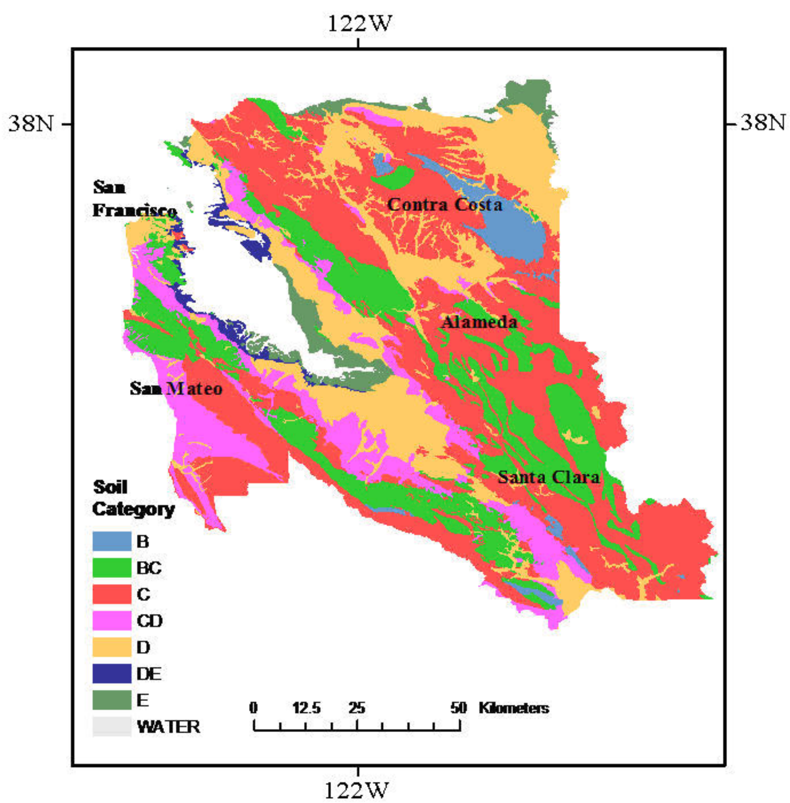

Fig. 3.2 NEHRP soil classes in San Francisco Bay Area (from NEHRP 2000).

3.2.1 Transportation Network Selection

The Metropolitan Transportation Commission San Francisco Bay Area highway network is used in the analyses of this study. It represents the major roads of the street network and it is mainly used for analysis and planning purposes. Although it does not fully reflect the geometry of the streets, it includes all their characteristics, such as direction, capacity, free flow speed, connectivity, and length.

The network is defined by a set of nodes and links. The nodes consist of locations where two or more highways intersect (usually interchanges), as well as locations where a highway crosses the boundary of the study area. Links are defined by lines (not self-intersecting) between two nodes with no other nodes in between. The link characteristics are described by free flow speed and flow capacity. The MTC network representation consists of 29804 links and 10647 nodes. The links and the nodes of the Metropolitan Transportation Commission network are shown in Figure 3.3 below.

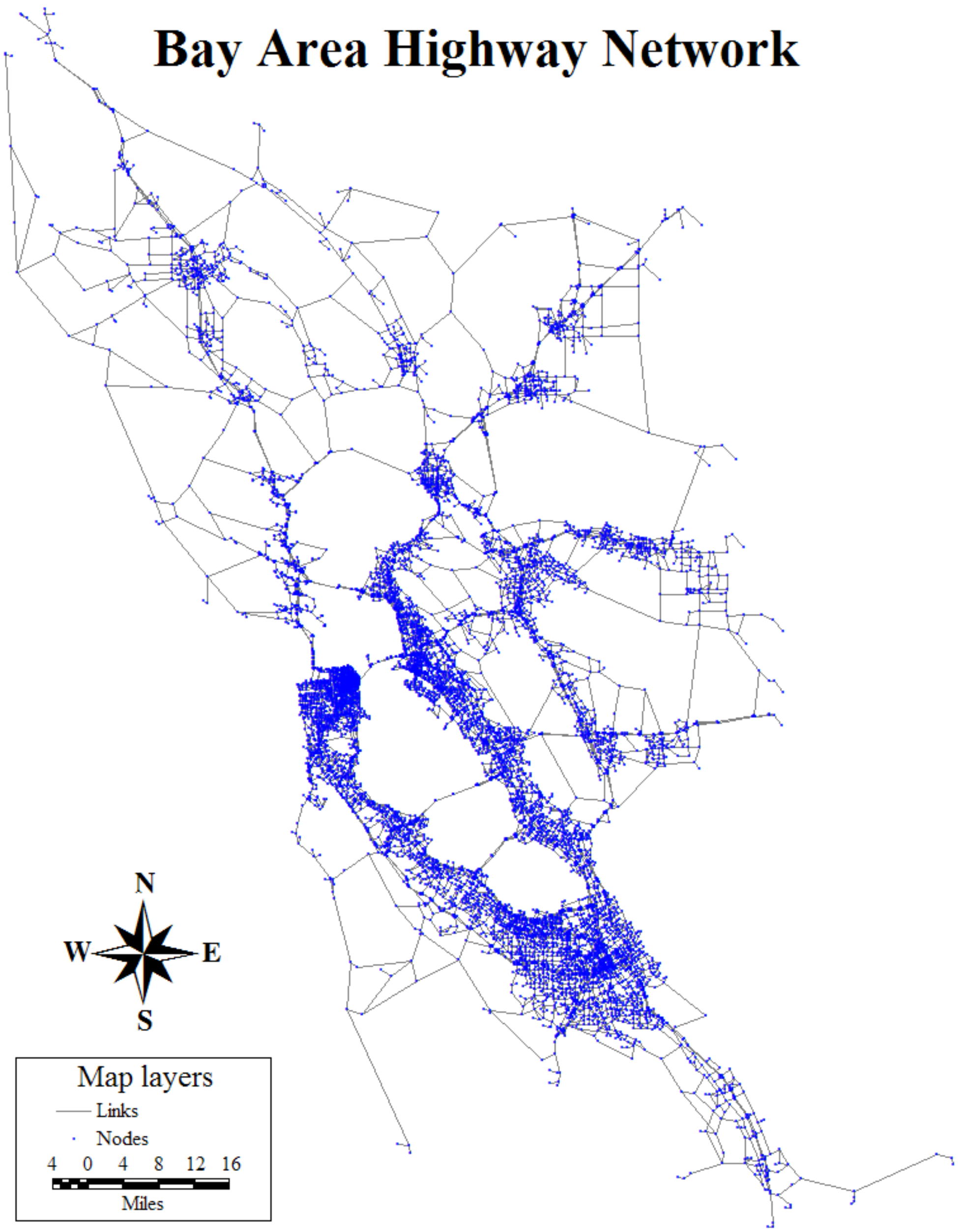

Fig. 3.3 Links and nodes of MTC network.

We consider 1120 Transportation Analysis Zones (TAZ) to account for both the intra- and inter-regional traffic. By definition, a TAZ is a geographic area that identifies land uses and associated trips that is used for making land-use projections and performing traffic modeling. It predicts the trip demand in that specific area based on the homogeneity of its population and its economic characteristics. The TAZs used in this study can be seen in Figure 3.4 below.

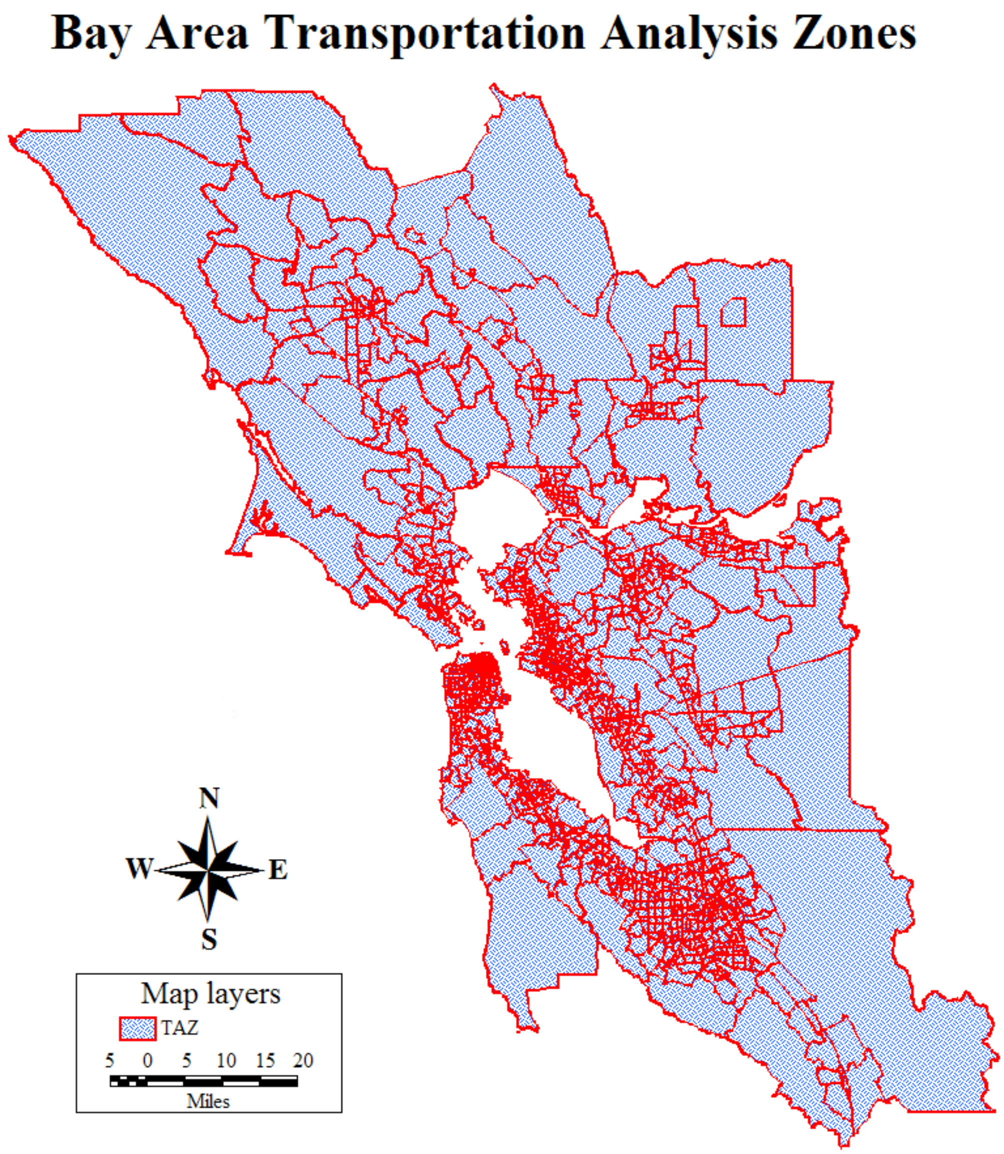

Fig. 3.4 Transportation analysis zones of Bay Area.

3.2.2 Origin-Destination Matrix Selection

The two-hour peak demand estimate for the Bay Area highway network is provided by the MTC, based on the 1990 household survey. It categorizes the trips according to their purpose (home-based–work, home-based–shop, home-based–social/recreation, home-based–school and non-home-based).

The two-hour peak demand matrix expresses the demand of the passengers during the peak hours. For our purposes, we need to assess the daily trips in the network to define the daily travel cost. In order to convert the two-hour peak demand to daily demand we have to define the scaling factor that expresses the daily traffic in terms of the peak hour traffic. Therefore, we consider the San Francisco Bay Area daily profile (Purvis, MTC 1999) of the demand, as shown in Figure 3.5 below, and compute the ratio of the demand of the trips during the two-hour morning peak demand to the total daily demand.

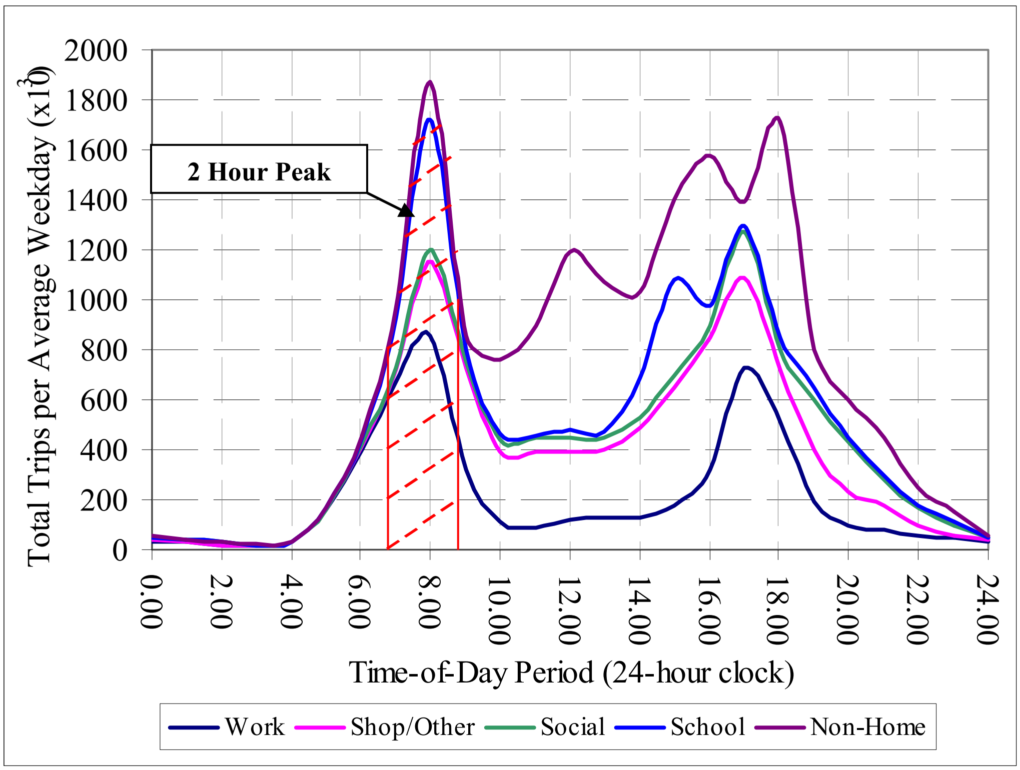

Fig. 3.5 Person trips by time of day and by trip purpose (from Purvis, MTC 1999).

The scaling factor based on the previous daily travel profile is equal to 5.40. This means that our total travel time estimate for the two-hour peak demand has to be multiplied by that scaling factor in order to estimate the daily total travel time.

Another assumption related to the origin destination matrix has to do with the vehicle car occupancy. The demand is expressed in passenger cars; therefore, we need to assume an average occupancy factor in order to estimate the number of passengers traveling. The reason for this conversion is that the operational loss can be computed based only on the man-hours lost; thus, the number of users is needed. We use vehicle car occupancy equal to 1.40 in all our analyses, as suggested by the Metropolitan Transportation Commission for the Bay Area (Caltrans 2002).

Finally, the value of time for the users of the Bay Area transportation network is assumed to be equal to $12.00/Hour. This hypothesis is in accordance with the California Life Cycle Analysis Model and is based on the socioeconomic profile of the Bay Area (Booz, Allen and Hamilton Inc. 1999).

3.2.3 Network Performance Measures

Our measure for the network performance is the total delay of the passengers of the network. This is defined as the increase in the total travel time caused by earthquake-induced damage. Essentially, it is the difference between the total travel time of the damaged network and the total travel time of the undamaged network. The total travel time is computed by the well known formula presented in Equation 3.1 and the total delay with Equation 3.2 below.

$$T = \sum_{\text{all links}} x_i t_i(x_i) \tag{3.1}$$

$$D = T_{before} - T_{after} = \sum_{\substack{\text{all links}\\ \text{before}}} x_i' t_i'(x_i') - \sum_{\substack{\text{all links}\\ \text{after}}} x_i t_i(x_i) \tag{3.2}$$

where

x_i is the flow on the link;

$t_i(x_i)$ is the travel time on link;

T_{before} is the total travel time before the event;

T_{after} is the total travel time after the event; and

D is the delay (and the primes refer to the parameters before the event).

The travel time on a link is calculated by utilizing a link performance function developed by the United States Bureau of Public Roads shown in Equation 3.3.

$$t_c = t_f \left(1 + a(\frac{V}{C})^{\beta} \right) \tag{3.3}$$

where

t_c is the congested link travel time;

t_f is the free flow link travel time;

V is the link volume;

C is the link capacity; and

a, β are calibration parameters, taken as 4 and 0.15, respectively, for the Bay Area.

The idea behind this adjustment of the link travel time is that after some users have chosen a specific link, it becomes less attractive to the other users. It is based on empirical data and that is why the calibration parameters a and β differ with location, time of day and road type.

3.2.4 Scenarios Considered for Estimation of Transportation Network Risk Curve

The earthquake sources that are taken into account are the events occurring on San Andreas and the Hayward faults. Uniform probability distributions are assigned to each fault, implying that earthquakes are equally likely to occur everywhere within these two source zones.

We only consider events greater than $M_w \geq 6.75$ for both faults and go up to 8.0 and 7.5 for the San Andreas and the Hayward fault, respectively, with magnitude step equal to 0.25. For each event, the rupture zone is assumed to take several different positions on the fault in order to catch the spatial uncertainty. The San Andreas and Hayward faults can be seen in Figure 3.6 below, while the events considered in this study are shown in Table 3.2:

Fig. 3.6 San Andreas and Hayward faults.

Table 3.2 Scenarios considered by moment magnitude and fault.

Fault	L_{fault}	M_w	$L_{rupture}$ (km)	N
San Andreas	235	6.75	28	9
San Andreas	235	7.00	43	9
San Andreas	235	7.25	66	8
San Andreas	235	7.50	100	6
San Andreas	235	7.75	153	4
San Andreas	235	8.00	235	1
Hayward	100	6.75	28	8
Hayward	100	7.00	43	6
Hayward	100	7.25	66	4
Hayward	100	7.50	100	1

In the previous table, all the scenarios considered for the generation of the risk curve are shown. For each scenario, *N* represents the number of events we simulate in order to account for the spatial uncertainty of the rupture. Thus, the loss for each rupture location will be different even though the magnitudes of the events are the same. The enumerated scenarios with the same intensity always move from south to north. A table with the exact location of the rupture zone of each scenario can be found in Appendix G. An example with the six different scenarios considered for the Hayward 7.00 event is shown below.

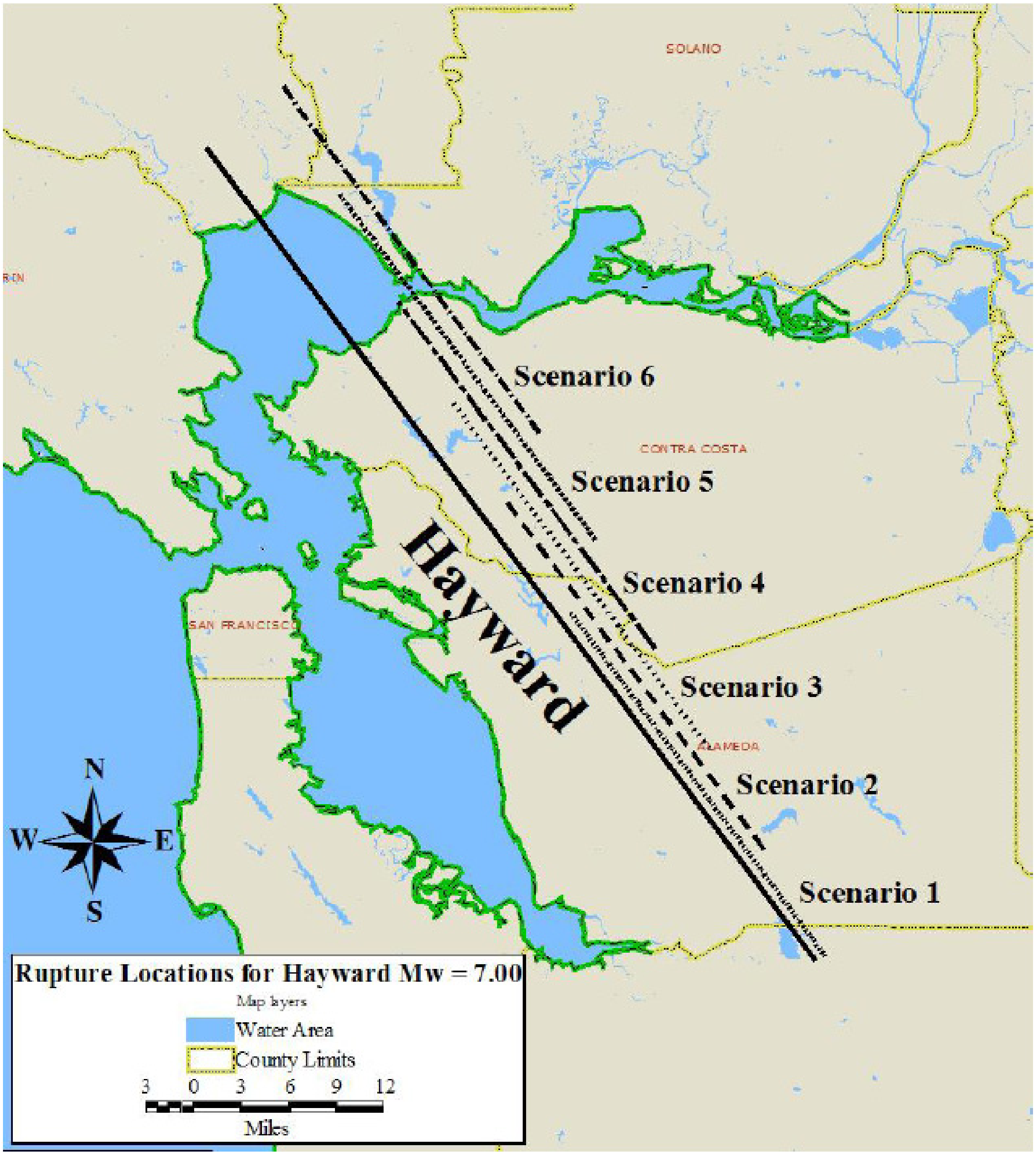

Fig. 3.7 Demonstration of rupture sliding along length of fault.

The annual rate of exceedance M_w = 6.75 for the San Andreas fault is equal to $v_{6.75}$ = 0.007, whereas for the Hayward fault is $v_{6.75}$ = 0.008. The parameter *b* is assumed to be equal to 0.68 and 3.2 for the same faults according to the USGS study (2003). A plot with the results of that study for the exceedance probabilities of moment magnitudes greater than 5.5 for the main faults in California follows.

We have assumed that ruptures along the fault corresponding to a particular magnitude have equal probability of occurrence. This assumption simplifies the model even though the rupture locations do not correspond to the characteristic event model presented in the USGS (2003) study. This simplification is introduced to make the risk computations for a large network system computationally tractable.

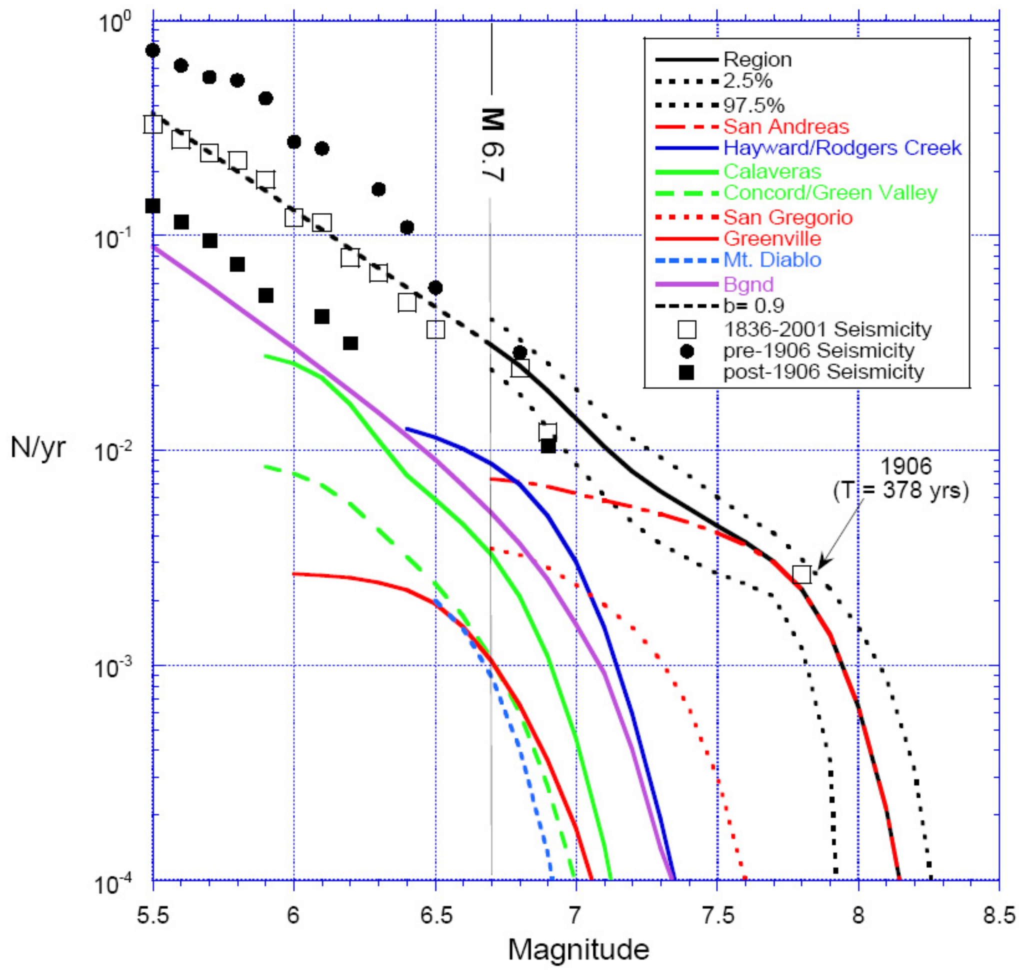

Fig. 3.8 Exceedance probabilities for main faults in California (from USGS 2003, Open File report 03-214).

In the previous plot, we can see that the Hayward fault annual rate decreases rapidly in the vicinity close to Mw = 7.25. This is the reason for the rather large value of the parameter b for that fault (b = 3.20). For the San Andreas fault, we can see that the slope is less than 45 degrees within the range M_w = 6.75 – 8.00 and is estimated as b = 0.68. The general equation for the bounded recurrence relationship is shown in Equation 3.4, while the modified equations for the two faults are presented in Equations 3.5 and 3.6, respectively:

$$\nu_m = \nu_{6.75} \frac{e^{-b*ln(10)*(m-M_{min})} - e^{b*ln(10)*(M_{max}-M_{min})}}{1-e^{b*ln(10)*(M_{max}-M_{min})}}, \quad M_{min} \leq m \leq M_{max} \tag{3.4}$$

$$\nu_{m,SA} = 0.007 \frac{e^{-1.28945(M-6.75)} - 0.19953}{0.80047}, \quad 6.75 \leq m \leq 8.0 \tag{3.5}$$

$$\nu_{m,HW} = 0.008 \frac{e^{-7.36827(M-6.75)} - 0.00398}{0.00602}, \quad 6.75 \leq m \leq 7.5 \tag{3.6}$$

where

β	is a parameter equal to *b*ln(10)*;
M_{min}, M_{max}	are the minimum and the maximum moment magnitudes considered in this study;
$\nu_{6.75}$	is the annual rate of occurrence of events with $M_w \geq 6.75$; and
ν_m	is the annual rate of exceeding any magnitude *m* within the range of 6.75 and M_{max}.

3.3 LOSS DUE TO STRUCTURAL DAMAGE OF NETWORK BRIDGES

The expected value of the structural damage of the bridges is computed for the 56 scenarios presented in Table 3.2. The reason why this type of analysis is chosen instead of the computation of the probability density function of the loss has to do with the size of our portfolio. Moreover, we only need to define the damage of each link to perform network analysis. The evaluation of the PDF of the loss will be demonstrated for a smaller network later in this chapter.

The total replacement cost of the 1125 bridges in the San Francisco Bay Area that are considered in this study is equal to \$2,891 M. The structural damage varies from \$0 to \$1,180 M for the San Andreas and from \$225 to \$1013 M for the Hayward fault. Plots with the expected value and standard deviation of the structural loss from the different faults follow.

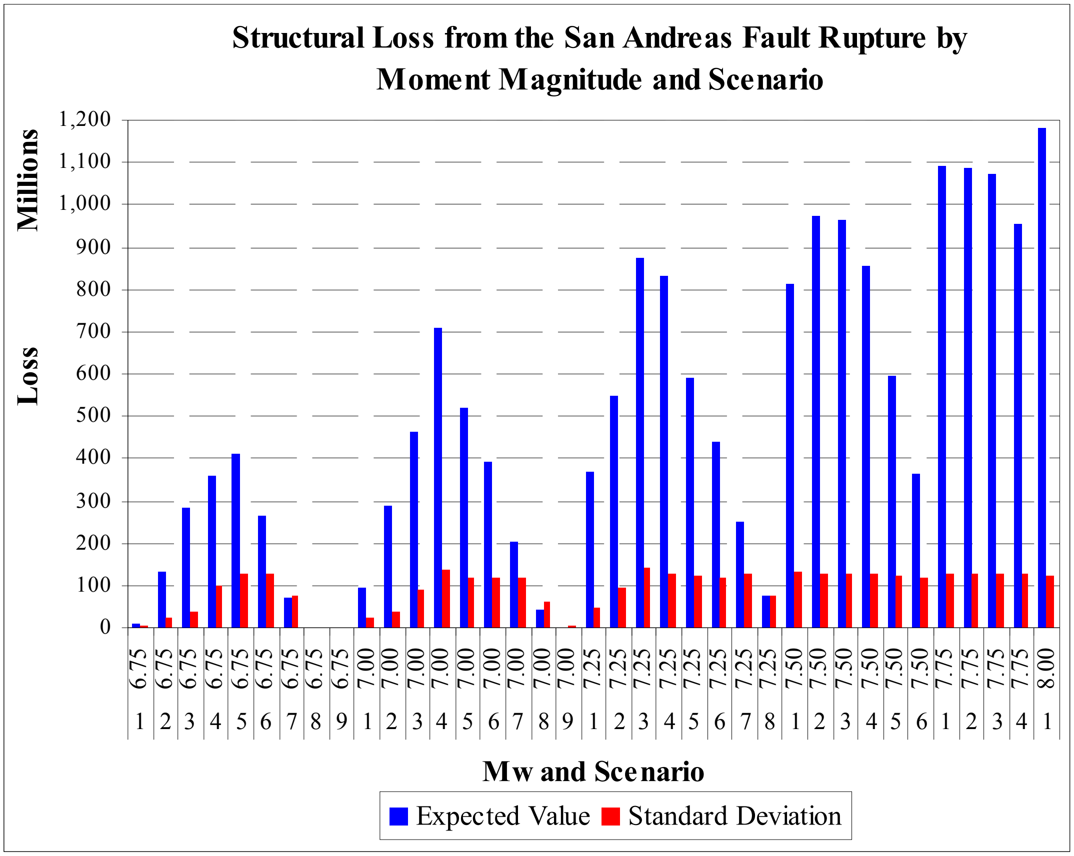

Fig. 3.9 Structural loss from San Andreas fault rupture.

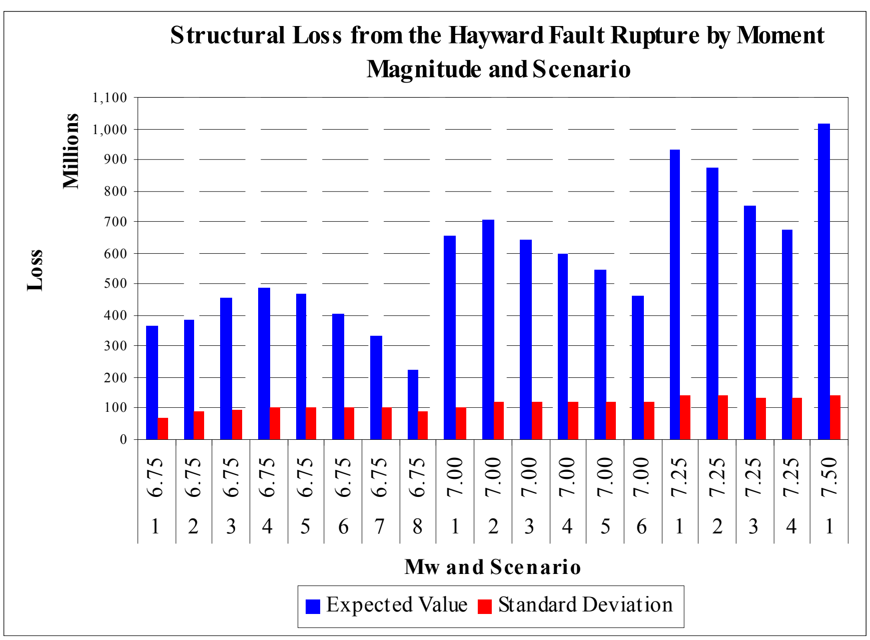

Fig. 3.10 Structural loss from Hayward fault rupture.

The structural loss estimates vary with the location of the rupture, especially for the San Andreas fault. This variation can be attributed to the geometry of the fault because rupture zones can be very far from the Bay Area.

The structural loss caused by the Hayward fault events seems to have smaller variation, probably because Hayward is located in the heart of the network. Moreover, a seismic event in the Hayward fault causes greater damage than an event in the San Andreas fault with the same moment magnitude.

Among the three hazards, ground shaking, liquefaction and landslide, we can say that liquefaction governs in the Bay Area. Ground shaking is the second most important failure mode while landslides do not seem to occur. Of course, these results strongly depend on the methodologies used for the computation of the damage and the authors are aware that the HAZUS (1999) methodology for the estimation of the ground failure is very conservative. A chart with the expected values and the standard deviations of the losses, categorized by the different hazards follows.

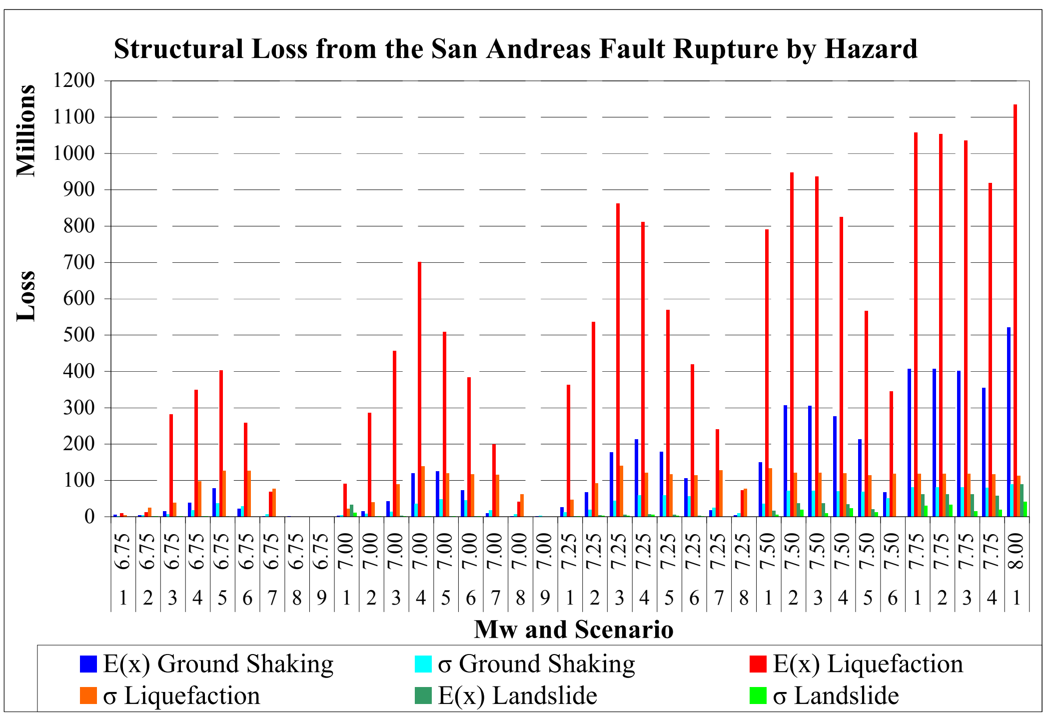

Fig. 3.11 Structural loss from San Andreas fault rupture by hazard.

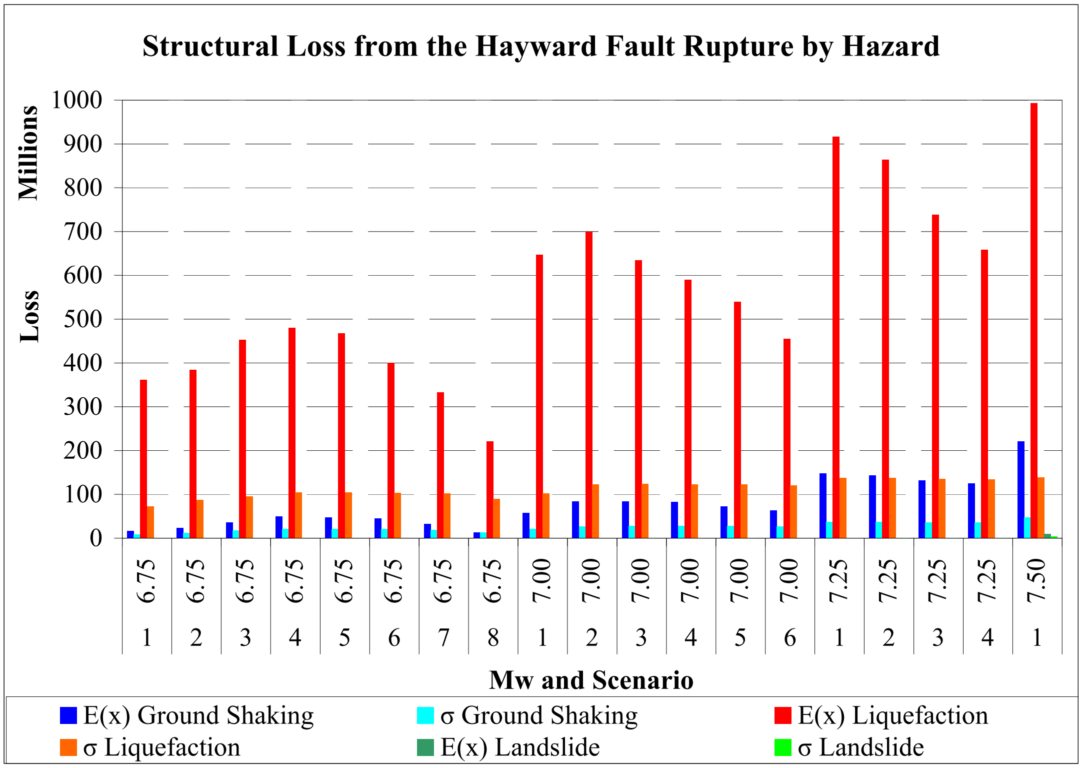

Fig. 3.12 Structural loss from Hayward fault rupture by hazard.

Based on this analysis, the loss due to liquefaction is significantly greater than the losses from the other two hazards. This trend is definitely correlated with the poor soil of the Bay Area, however, we believe that further investigation is needed before we can rely on these results. The loss from ground shaking is proportional to the loss from liquefaction and is usually between 30% and 50%. Loss from landslides is rather small in all the scenarios investigated, independently of the rupture location and moment magnitude. This behavior does not necessarily mean that earthquake-induced landslides are not possible in the Bay Area. Small losses from landslides result most likely because the methodology does not predict landslides reliably at bridge locations.

Overall, our loss estimates increase with magnitude and decrease with distance. For the same level of intensity, the Hayward fault leads to higher losses than the San Andreas fault because of its location. As observed, the San Andreas fault can cause the maximum structural loss, equal to $1.1B.

3.4 LOSS DUE TO NETWORK DISRUPTION

For each of the events considered, the loss due to the disruption of the San Francisco Bay Area Highway Network is estimated. The expected damage of each link is used to account for its reduced capacity. In case the damage exceeds 40%, the link is assumed to be closed until the damage is repaired. The daily operational loss is then converted to monetary units by multiplying the total daily delays with the assumed value of time ($12.00/Hour per passenger).

In order to estimate the total losses over time, we perform six network analyses corresponding to 1, 3, 7, 14, 30, 180, and 365 days after the event has occurred. If we assume linear decrease of the daily loss between the days computed, we can construct a plot of the change of the daily loss over time. The total operational loss is then computed through integration of that curve. The change of the daily loss is plotted below for three selected cases.

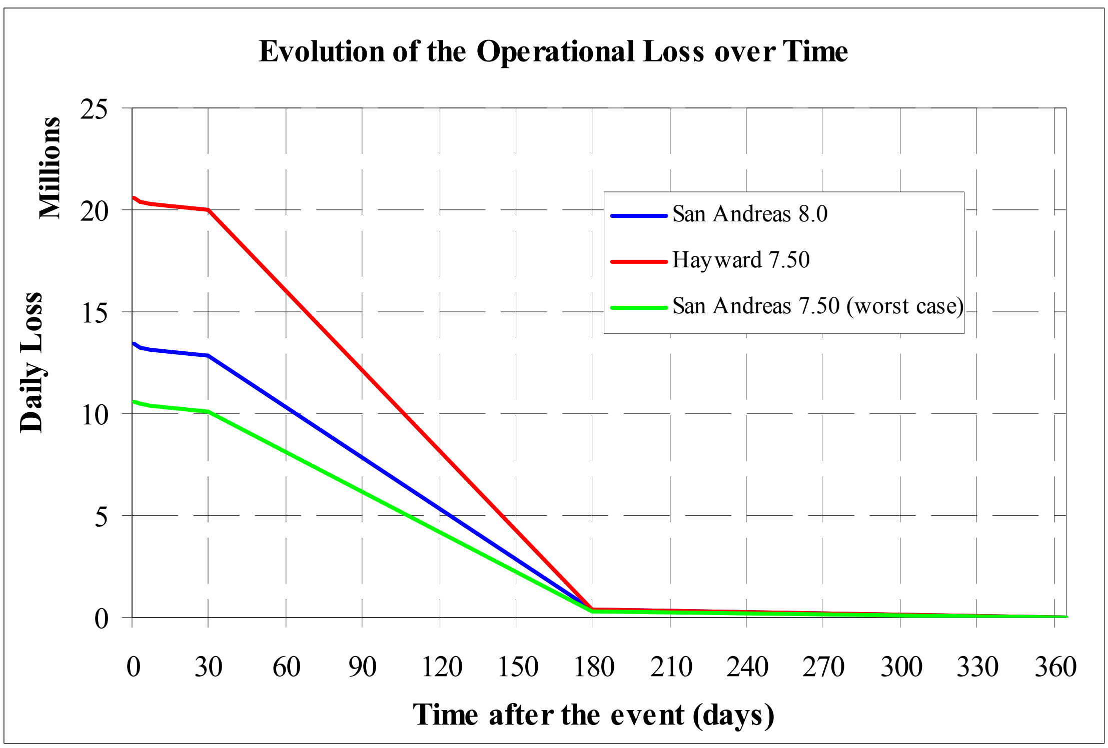

Fig. 3.13 Evolution of operational loss over time for three scenarios.

In the previous plot we have the evolution of the daily loss for the San Andreas 7.50 and 8.00 and the Hayward 7.50 scenarios. We can see that the daily loss from the Hayward 7.50 scenario is always higher than the other two daily losses. Another interesting observation is that the San Andreas 8.00 daily loss does not differ significantly from the daily loss caused by a scenario with moment magnitude equal to 7.50 in the same fault. This implies that the damage caused by the rupture of the San Andreas fault is not very sensitive to the moment magnitude.

By repeating the same procedure for all the investigated events, we compute the total operational loss of each event. Graphs with the operational losses from rupturing in the different faults follow.

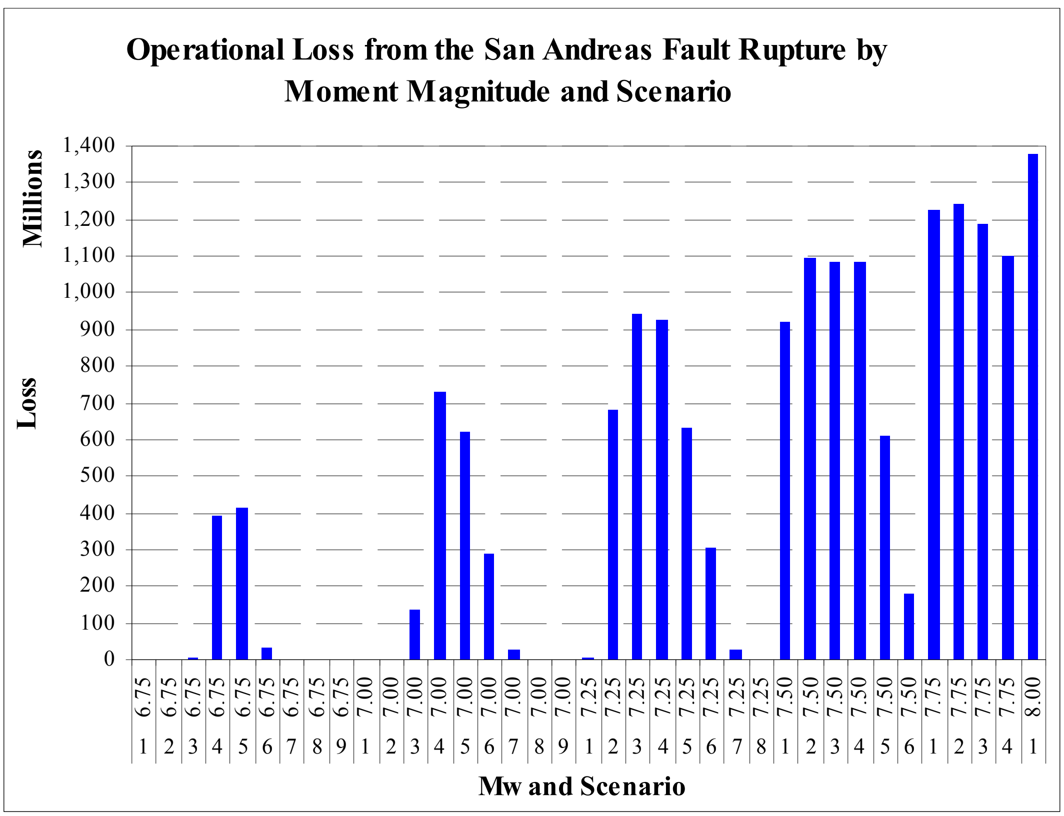

Fig. 3.14 Operational loss from San Andreas fault rupture by moment magnitude and scenario.

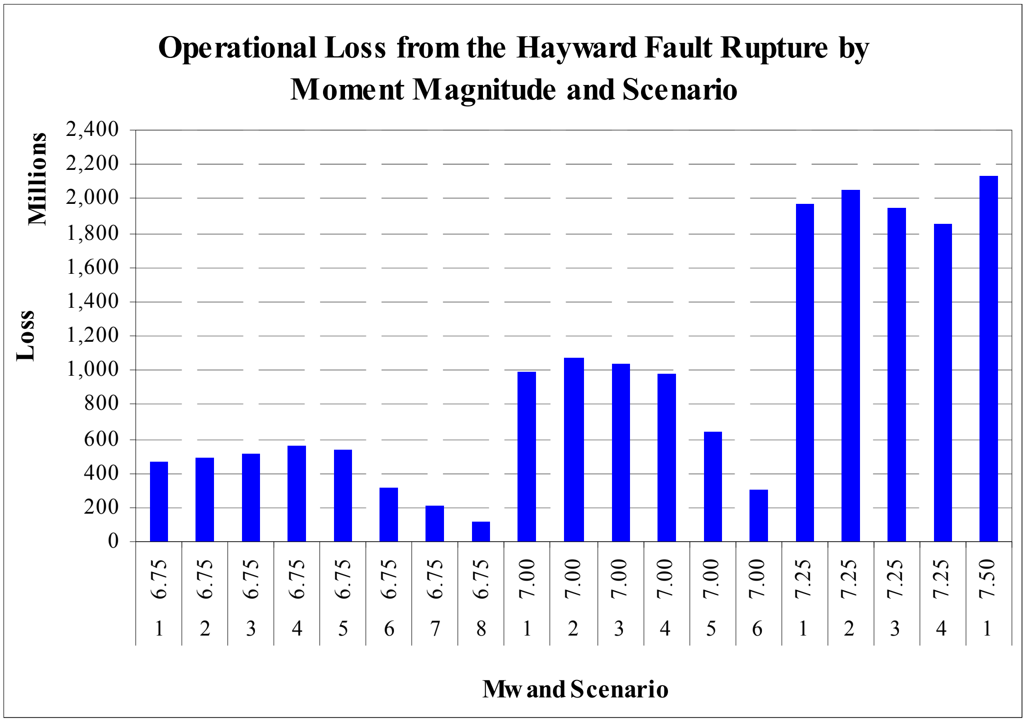

Fig. 3.15 Operational loss from Hayward fault rupture by moment magnitude and scenario.

The operational loss varies from 0 to $1,380 M for the San Andreas fault and from $110 to $2,120 M for the Hayward. Again, the Hayward fault causes more severe losses to the transportation network than the San Andreas fault, even for the smaller moment magnitude of its events.

The estimated losses are for the fixed-demand case, where we assume that the demand remains constant after the earthquake event. It should also be clarified that the previous losses only reflect the losses due to commuter traffic delays and not due to freight traffic. *If freight traffic had been considered, the operational loss would further increase, since freight trips are five to six times more expensive than the passenger trips.*

Another important remark in the study of the operational loss is that it reflects the network damage caused by the 1125 bridges considered. If additional data were available and we were in position to model all the bridges of the Bay Area transportation network including the street network, our estimations for the operational loss would most likely change.

3.5 AGGREGATION OF STRUCTURAL AND OPERATIONAL LOSS

The structural and the operational losses are summed in order to estimate the total loss for each event. Again, it should be mentioned that the results below reflect only the losses due to commuter traffic delays. The aggregated losses for the different events are shown below.

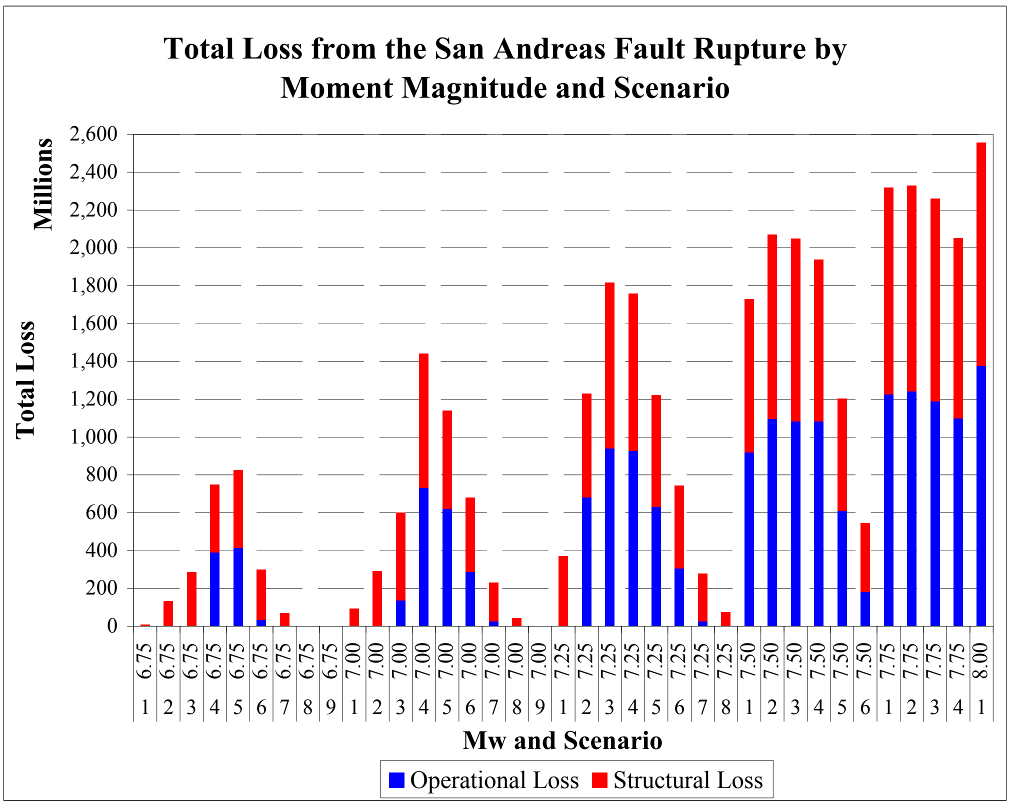

Fig. 3.16 Total loss from San Andreas fault rupture by moment magnitude and scenario.

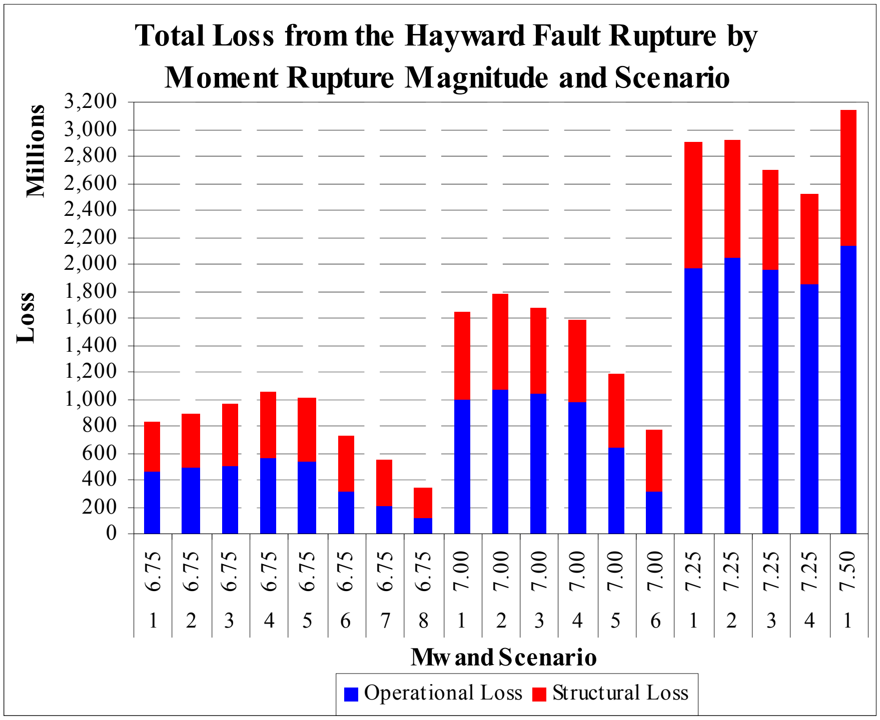

Fig. 3.17 Total loss from Hayward fault rupture by moment magnitude and scenario.

For the San Andreas fault the operational loss is very close to the structural, unlike the Hayward events where the operational loss governs. Again, this difference can be attributed to the spatial distribution of the network relative to the two faults and the fact that the Hayward fault crosses many of the ACT zones.

3.6 ANNUAL RISK CURVE FOR SAN FRANCISCO BAY AREA TRANSPORTATION NETWORK

Risk curves are a useful mean to convey information to decision makers regarding the overall risk of the system. Such curves express the probability of exceeding a specific value and are widely used in civil engineering. In this study we present the annual risk curve of the aggregated loss of the San Francisco Bay Area transportation network due to the seismic hazard from San Andreas and Hayward. With the term aggregated loss we denote the structural and the operational loss.

The concept we use is straightforward. We assume that no events can happen at the same time (which is reasonable given that we consider rare large events), and we treat the probabilities of each of the events to occur as realizations of the PDF of the loss. In this way we obtain the following curve.

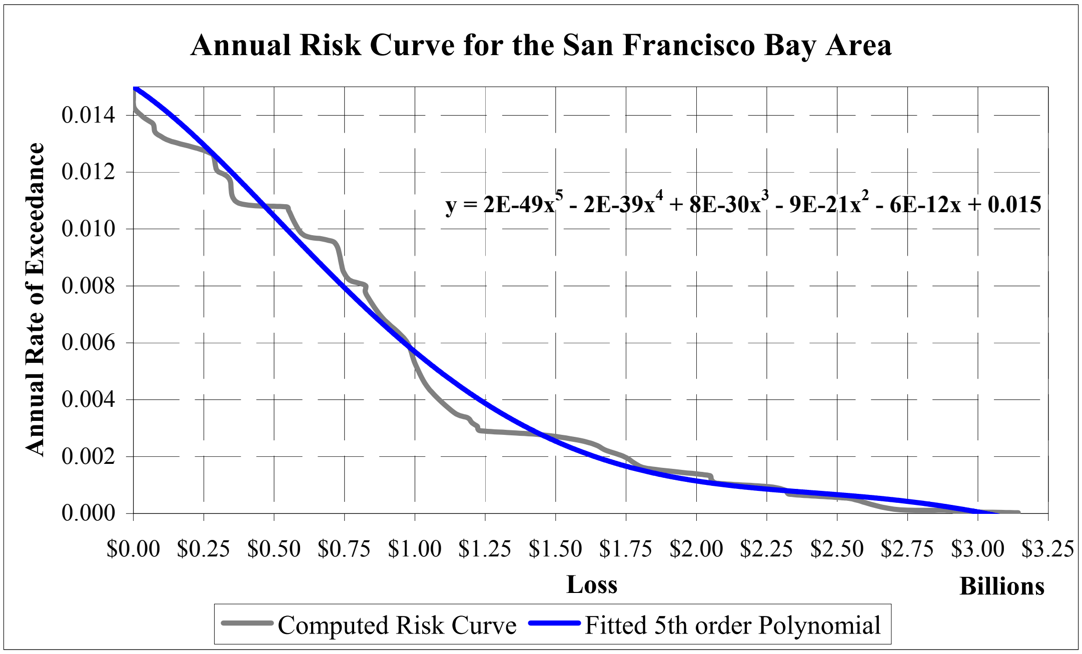

Fig. 3.18 Annual risk curve for transportation network.

The total losses can reach \$3.1 B, whereas the expected value of the annual risk is \$13.3 M. Thus, a decision maker can reduce the risk (e.g., insurance) by spending this amount in mitigation annually. This kind of cash flow is a perpetuity with annual payment of \$13.3 M and its present value (PV) is computed using Equation 3.7:

$$PV_{perpetuity} = \lim_{T \to \infty} \sum_{i=1}^{T} \frac{C}{(1+r)^i} = \frac{C}{r} \tag{3.7}$$

where

PV is the present value of the perpetuity;

T is the time of the last payment;

C is the amount paid every year; and

R is the effective interest rate.

The effective interest rate in Equation 3.7 is very difficult to predict; therefore, we present a plot with the sensitivity of the present value of the annual risk to that parameter below.

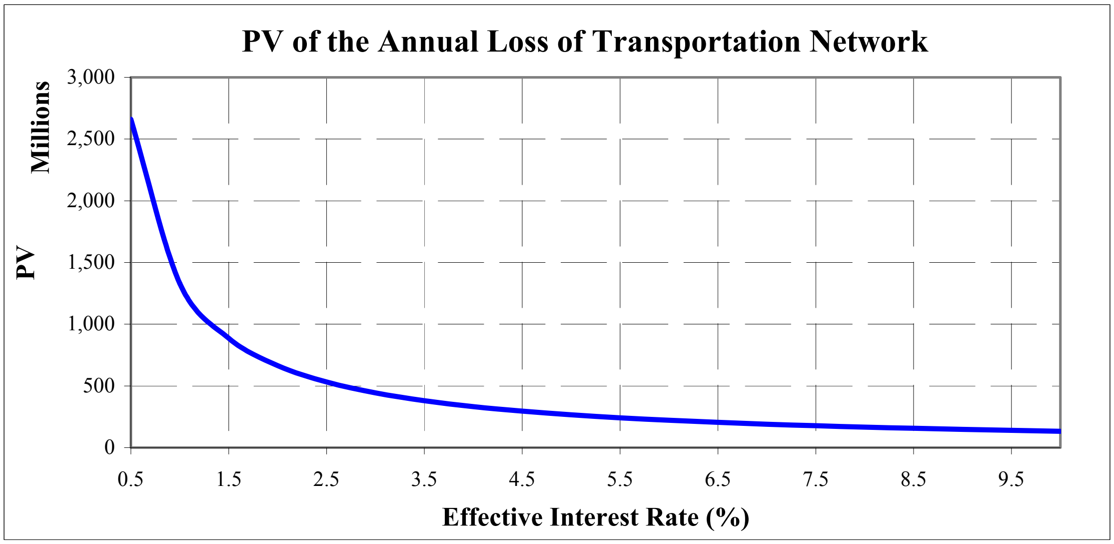

Fig. 3.19 Present value of annual risk vs. effective interest rate.

From this figure, we can see that the potential loss of the transportation network studied varies from \$150 to \$2,650 M (structural and operational loss due to commuter traffic). This is a very useful conclusion for retrofitting and planning purposes, since it enables decision makers to quantify the risk of the transportation system. For example, if we assume that the transportation network disruption will not cause any other type of losses (business downtime, casualties etc), a retrofitting strategy that costs more than the estimated potential loss, should be rejected simply because society will choose to keep the risk.

3.7 DEMONSTRATION OF ASSESSMENT OF PROBABILITY DENSITY FUNCTION OF STRUCTURAL LOSS FOR PORTFOLIO OF TEN BRIDGES

The methodology we propose for the evaluation of the distribution of the structural loss of a portfolio of bridges after an earthquake event is presented in this section for demonstration purposes. Several cases are examined. First, we estimate the PDF of the structural loss without considering the uncertainties of the replacement cost and the damage factor. Then we assume variable replacement cost and variable damage factor separately. Finally, we account for all the uncertainties introduced at the same time.

We select ten bridges in South San Francisco on Highway 101 and assume that the San Andreas 8.0 event occurs. We then estimate the distribution of the loss of all those bridges individually and aggregate it through convolution. The total replacement cost for the ten bridges is \$29.8 M. A description of the selected bridges and their properties can be found in Table 3.3 below, while the generated loss curves follow.

Table 3.3 Bridges selected for demonstration.

	BRIDGE ID	NAME	LOCATION	VALUE
1	35 0130	SIERRA POINT OVERHEAD	04-SM-101-23.66-BSBN	\$7,948,248
2	35 0130S	SIERRA POINT OFF-RAMP OH	04-SM-101-23.66-BSBN	\$2,749,725
3	35 0131S	SIERRA POINT OFF-RAMP OC	04-SM-101-23.39-SSF	\$1,123,122
4	35 0094L	SOUTH SAN FRANCISCO OH	04-SM-101-21.92-SSF	\$5,269,880
5	35 0094R	SOUTH SAN FRANCISCO OH	04-SM-101-21.92-SSF	\$4,644,640
6	35 0121	SOUTH SF BELT RAILWAY OH	04-SM-101-21.80-SSF	\$2,343,000
7	35 0119	COLMA ROAD UC	04-SM-101-21.69-SSF	\$2,221,110
8	35 0118	COLMA CREEK	04-SM-101-21.61-SSF	\$1,929,840
9	35 0281F	NORTH CHANNEL(W380-N101)	04-SM-380-6.48-SBR	\$583,200
10	35 0261R	7TH AVE UC	04-SM-380-6.20-SBR	\$1,021,680
			TOTAL	\$29,834,445

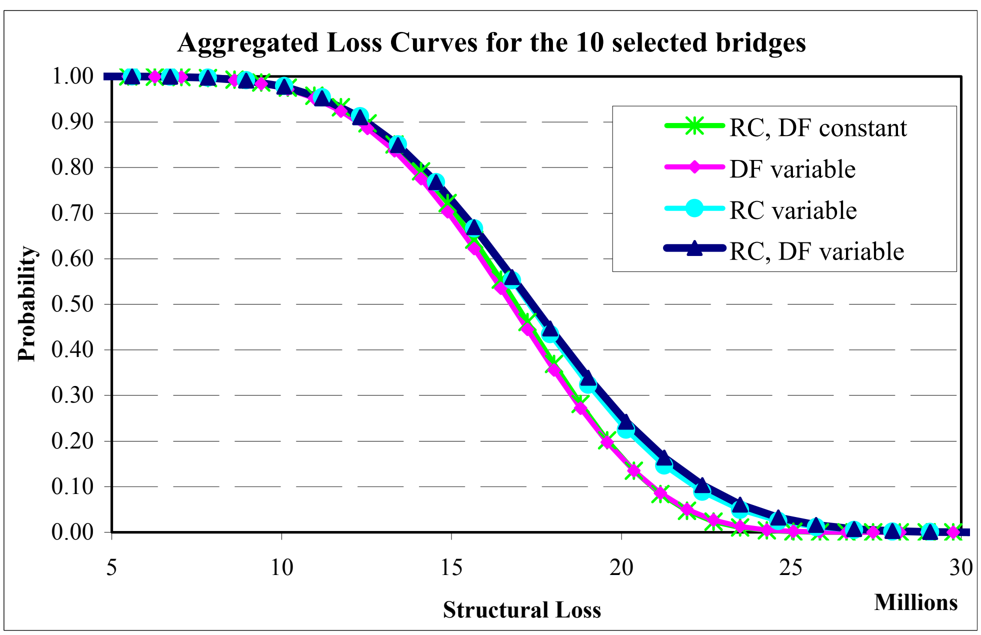

Fig. 3.20 Aggregated loss curves for 10 bridges.

If we compute the loss curve without considering any of the uncertainties we introduce, we obtain the green curve for the aggregated loss with μ_x = \$16.8 M and σ_x = \$4.4 M. When we assume that the damage factor (DF) is variable only within the limits suggested by HAZUS (1999), we compute the purple curve with μ_x = \$16.7 M and σ_x = \$4.4 M. In case the Replacement Cost is considered as a truncated normal random variable, the expected value of the loss becomes μ_x = \$17.4 M and σ_x = \$5.1 M. Finally, if we assume that both the uncertainties in the RC and the DF are present, the expected loss becomes μ_x = \$17.5 M and σ_x = \$5.0 M.

Our results indicate that the consideration of the uncertainty in the replacement cost results in higher risk estimations, especially in the vicinity of \$20 M. On the other hand, when the damage factor is modeled as a random variable, it does not seem to change our estimates. In case we consider the two uncertainties present at the same time, the estimated risk level increases but this happens mostly due to the consideration the replacement cost uncertainty.

In order to further investigate the influence of the uncertainty in the damage factor, a few more cases are examined. The additional analyses assume a wider interval of the possible values of the damage factor for each damage state and keep the same mean value resulting in larger dispersion. A table with the new limits of the damage factors and the loss curves that correspond to those limits follow.

Table 3.4 Limits of damage factor by damage state (modified by HAZUS).

HAZUS Damage State	Central Damage Factor	Minimum Damage Factor	Maximum Damage Factor	δ	N
None	0.00	0.00	0.00	0.00	-
Slight	0.03	0.01	0.06	0.30	0.986
Moderate	0.08	0.04	0.20	0.30	0.952
Extensive	0.25	0.12	0.45	0.30	0.955
Complete	0.70	0.30	1.00	0.30	0.895

In the previous table, δ, represents the coefficient of variation and N the normalization factor for the truncated normal distributions.

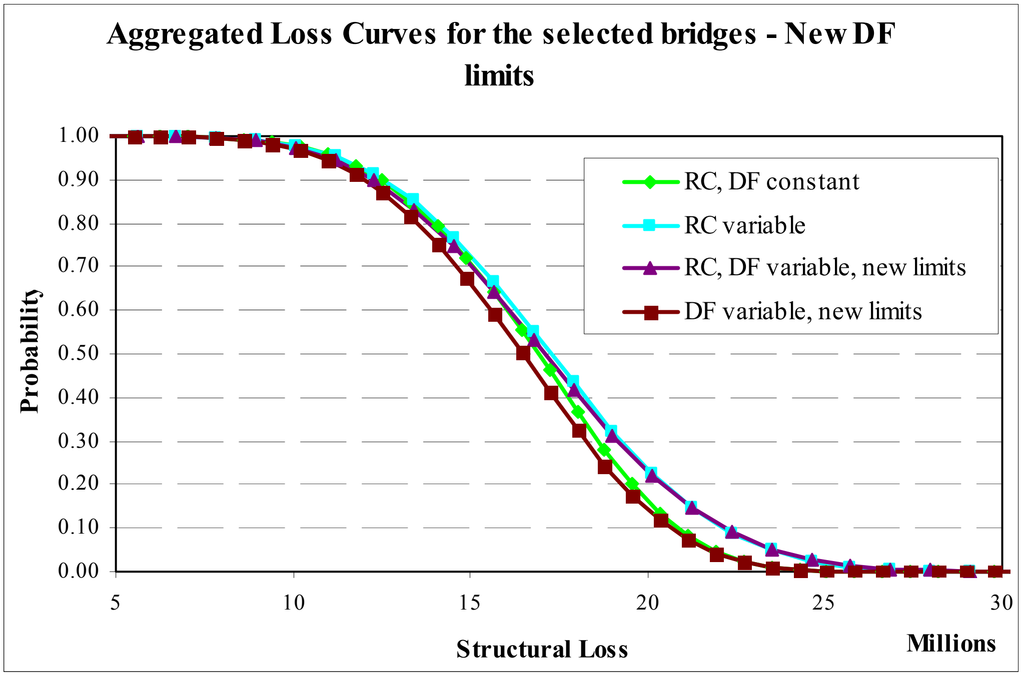

Fig. 3.21 Aggregated loss curves for enhanced damage factor limits.

Even with a wider range of possible values, the damage factor does not affect the complementary cumulative distribution function when considered together with the replacement cost uncertainty (purple curve). When considered alone, it seems to slightly reduce the probability of exceedance estimates.

The reason for the slight reduction of the loss curve when considering variable damage factors is because the damage factor is spread over a wider range and is related to the shape of PDF we assume for them. Particularly, the truncated normal distributions we assume, are not truncated symmetrically but tend to have a longer tale towards higher values of the damage factor. Consequently, the density is gathered towards the lower values and this does not change when we multiply with the normalization factor *N*. The result is a distribution skewed to the left that slightly decreases the loss curve.

The previous results imply that the replacement cost uncertainty has a greater influence on the loss estimates and can lead to a significant increase of the probability of exceedance. Damage factor variation does not seem to play an important role in the estimation of the aggregated loss and results to slightly lower loss estimations.

4 Summary and Conclusions

4.1 SUMMARY

A method is developed for the risk assessment of transportation networks that not only accounts for the structural loss of the bridges of the network, but also for the operational loss due to network disruption. The structural loss is computed based on HAZUS (1999). The operational loss is computed based on the total delays after the seismic event, until the transportation network is fully repaired.

The annual risk curve of total losses of the Bay Area transportation network (structural and operational) is developed for the earthquake hazards of the San Andreas and Hayward faults. We account for moment magnitudes from 6.75 to 8.00 and 6.75 to 7.50 on the San Andreas and the Hayward fault, respectively, and account for 56 events in total.

Formulations of structural loss that include uncertainties in the replacement cost and the damage factor are presented. We assume that the losses for the individual bridges are independent and apply the convolution density formula to obtain the distribution of the total loss of a portfolio of bridges after a seismic event. All prior assessments of portfolios of bridges provide only the expected value of the loss and not the PDF.

4.2 CONCLUSIONS

Two types of analyses are performed in this study. Estimation of the loss due to structural damage and estimation of the loss due to transportation network disruption. The major observations from our analyses were:

The structural loss estimates for the 1125 pre-retrofitted bridges that were identified in the network varied with the moment magnitude and the location of the fault. In particular, for the San Andreas fault the structural loss could be in the order of a few thousands for an event in the northern segment with $M_w = 6.75$ and reach \$1,200 M for the $M_w = 8.0$ event. For the Hayward fault, the minimum structural loss is \$ 225 M for the $M_w = 6.75$ event and the maximum loss is \$1,013 M for the $M_w = 7.50$ event.

From the three hazards considered in this study, liquefaction, ground shaking, and landslide, liquefaction was the main cause of failure. Specifically, it contributed more than 90% of the structural loss in all the scenarios investigated and was eight or nine times greater than the loss caused by ground shaking. Although this may be true in reality, the authors believe that it is a result of the methodology used to predict the damage from ground failure. In particular, the fragility functions proposed by HAZUS (1999) appear to be overly conservative; hence, the estimated damage appears to be very high.

In the computation of the PDF of the loss of a single structure, consideration of the uncertainty in the replacement cost results in an increase of the risk that can be 75% higher than when it is modeled as a constant. The reason for this change is that the introduction of variability in the RC increases the variance of the loss. At the same time, consideration of the uncertainty in the damage factor slightly decreases the risk. This behavior is most likely related to the asymmetric shape of the truncated normal distributions used to model this uncertainty. The asymmetry is caused by the fact that the central damage factor of each damage state does not have symmetric bounds but is skewed to the left; thus lower damage factor values weigh more after the truncation normalization.

The convolution proposed for the estimation of the PDF of the aggregated loss of a set of bridges (convolution) reveals more information to the decision makers than the expected value estimates. In particular, the shape and the higher order moments of the distribution of the loss can be evaluated, in addition to its expected value as demonstrated through the application to ten bridges.

Based on the mean repair times suggested by HAZUS (1999), the operational loss can reach \$1,376 M for the San Andreas $M_w = 8.0$ event and \$2,129 M for the Hayward $M_w = 7.50$ event. The estimates are on the average 62% and 146% of the structural loss of the San Andreas and the Hayward scenario events, respectively. In general, structural loss governs in the small magnitudes and as we move to higher magnitudes, the operational loss governs. It should be noted that our operational loss estimates do not include the freight traffic trips and the authors believe that such a consideration would further increase the losses.

Our results indicate that events in the Hayward fault cause more severe structural and operational losses than events in the San Andreas. This trend is counterintuitive because of the higher moment magnitudes that the San Andreas events can have compared with the Hayward events. Nevertheless, a careful look at the map of the Bay Area will reveal the strategic position of the Hayward fault in the heart of the Bay Area transportation network. In other words, although the San Andreas fault causes higher structural damage, the Hayward fault governs because of its more important consequences to the transportation network.

The annual probability of loss exceedance curve developed for the Bay Area transportation network increases significantly with consideration of the operational loss. The expected annual loss for the transportation network is \$13.3 M. The present value of this risk depends on the future value of money implied by the effective interest rate and was found to vary from \$200 to \$2,500 M for interest rates between 10% and 0.5% respectively.

4.3 FUTURE RESEARCH

Undoubtedly, there are several areas of further research that would help towards the estimation of the structural and the operational loss of transportation systems. First, we believe that more accurate methods for the estimation of the structural loss are needed, especially for the damage due to ground failure. We lack practical methodologies to describe the liquefaction hazard, while the fragility functions that describe the vulnerability of the bridges due to that hazard are very conservative.

Second, we believe that the case where adjacent sites have correlated losses needs to be examined. In the current study, all the loss estimates for multiple bridges are based on the assumption that individual losses are independent. Bridge losses are likely to be correlated because ground motions and bridge performance of similar bridges are correlated.

Equally important is the focus on the estimation of the PDF of the loss of an individual bridge or a portfolio of bridges. Expected value loss estimates carry limited information. Thus, the performance of bridges of different risk levels is best represented by a probability density function.

Regarding the network analysis part, the variable-demand model in the traffic assignment should be investigated in addition to the fixed-demand model that is used in the current study. Also, post-event emergency traffic needs to be explored by future researchers and has to be incorporated in the post-event trip demand.

References

Association of Bay Area Governments (ABAG), 1997, Riding Out Future Quakes - Pre-Earthquake Planning for Post-Earthquake Transportation System Recovery in the San Francisco Bay Region, ABAG Publications

Basoz, N., and Kiremidjian, A.S., 1999, *Evaluation of Bridge Damage Data from Recent Earthquakes*, Earthquake Spectra, Vol. 15 (1).

Basoz, N., and Mander, J., 1999, *Enhancement on the Highway Transportation Lifeline Module in Hazus*, National Institute of Building Sciences, Draft 7.

Basoz, N., and Kiremidjian, A.S., 1999, *Development of empirical fragility curves for bridges*, ASCE Technical Council, Monograph N. 16, W. M. Elliott and P. McDonough, eds., ASCE, Reston, Va.

Basoz, N., and Kiremidjian, A.S., 1996, *Risk Assessment for Highway Transportation Systems*, PhD. Dissertation submitted to the Department of Civil Engineering, Stanford University

Beckman, M.J., McGuire, C.B. and Winsten, C.B., 1956, *Studies in the Economics of Transportation*, Cowles Commission Monograph, New Haven, Conn.: Yale University Press.

Boore, D., Joyner, W., and Fumal, T., 1997, Equations for Estimating Horizontal Response Spectra and Peak Acceleration from North American Earthquakes: A Summary of Recent Work, Seismic Research Letters, 687(1), 128-154.

Booz Allen & Hamilton Inc., 1999, *California Life Cycle Benefit/Cost Analysis Model*, California Department of Transportation.

California Department of Transportation, 2002, 2000-2002 California Statewide Household Travel Survey.

Caliper Corporation, 2004, Transcad Software Technical Manual

Cho, S., Fan, Y.Y., and Moore, J., (2003), *Modeling Transportation Network Flows as a Simul-*

taneous Function of Travel Demand, Network Damage, and Network Level of Service, the Proceedings of the ASCE Technical Council on Lifeline Earthquake Engineering (TCLEE) Sixth U.S. Conference and Workshop on Lifeline Earthquake Engineering, August 10-13, 2003, Long Beach, CA, pp. 868-877

Cornell, A., and Krawinkler, H., 2000, *Progress and challenges in seismic performance assessment,* PEER Center News, 3 (2), Pacific Earthquake Engineering Research Center, University of California, Berkeley

Federal Highway Administration, 1996, *Recording and Coding Guide for the Structural Inventory and Appraisal of the Nation's Bridges*, Report No: FHWA-PD-96-001, Office of Engineering Division, Federal Highway Administration, U.S. Department of Transportation, [http://www.fhwa.dot.gov/bridge/bripub.htm].

Frank, M., and Wolfe, P., 1956, *An Algorithm for Quadratic Programming*, Naval Research Logistics Quarterly, Volume 3, pp. 95-110.

HAZUS, 1999, *Earthquake Loss Estimation Technical Manual*, National Institute of Building Sciences, Washington D.C.

He, R., and Kornhauser, A.L., 2006, *Essentially Bet Routes in Dynamic and Stochastic Transportation Network*, International Journal of Vehicular Information and Communication Systems (in press)

Heidtman, K., Skarpness, B., and Tornow, C., 1997, *Improved Vehicle Occupancy Data Collection Methods, Final Report*, Office of Highway Information Management 1994-1997, Federal Highway Administration, Washington, DC 20590

Highway Research Board, *Highway Capacity Manual 1965, Special Edition 87*, Highway Research Board, National Academy of Science-National Research Council, Washington, D.C.

Kiremidjian, A.S., Moore, J., Fan, Y.Y., Basoz, N., Yazali, O., and Williams, M., 2003, *Pacific Earthquake Engineering Research Center Highway Demonstration Project*.

Kramer, Steven L., 1996, *Geotechnical Earthquake Engineering*, Prentice Hall.

Mackie, K., and Stojadinovic, B., 2001, *Probabilistic Seismic Demand Model for California Highway Bridges*, Journal of Bridge Engineering, Vol. 6, No. 6

Mackie, K., and Stojadinovic, B., 2004, *Fragility Curves for Reinforced Concrete Highway Overpass Bridges*, Proceedings of the 13th World Conference on Earthquake Engineering, Vancouver, BC.

Makdisi, F. I., and Seed, H. B., 1978, *Simplified Procedure for Estimating Dam and Embankment Earthquake Induced Deformations*, Journal of the Geotechnical Engineering Division, ASCE, Vol. 104, No. GT7, pp 849-867.

Moore, J.E., Little, R.G., Cho, S., and Lee, S., 2005, *Using Regional Economic Models to Estimate the Costs of Infrastructure Failures:* The Cost of a Limited Interruption in Electric Power in the Los Angeles Region, Keston Institute for Infrastructure, University of Southern California

Nielson, B. and DesRoches, R., 2004, *Improved Methodology for Analytical Fragility Curves for Bridges*, Proceedings of the Probabilistic Mechanics Conference, July 23-25, 2004

Priestley, M.J., Seible, F., and Galvi, G.M., 1996, *Seismic Design and Retrofit of Bridges*, (John Wiley and Sons).

Purvis, C., 1999*, Peak Spreading Models: Promises and Limitations*, 7th TRB Conference on Application of Transportation Planning Methods, Boston, Massachusetts

Sarabandi P., Pachakis D., King S., and Kiremidjian A.S., 2004, *Empirical Fragility Functions from Recent Earthquakes*, Proceedings of the 13th World Conference on Earthquake Engineering, Vancouver, BC, Canada. Paper No. 1211

Shinozuka, M., Murachi, Y., Dong, X., Zhou, Y., and Orlikowski, M.J., 2003, *Effect of Seismic Retrofit of Bridges on Transportation Networks*, Journal of Earthquake Engineering and Engineering Vibration, Vol. 2, No 2.

Shinozuka, M., 2000, *Development of Bridge Fragility Curves Based on Damage Data*, Earthquake Engineering and Engineer Seismology: An International Journal, Vol. 2, No. 2, pp 35-45.

Shinozuka, M., Feng, M.Q, Lee, J., and Naganuma, T., 2000, *Statistical Analysis of Fragility Curves*, ASCE Journal of Engineering Mechanics, Vol.126, No.12, pp 1224-1231

Shinozuka, M., Murachi, Y., Dong, X., Zhou, Y., and Orlikowski, M.J., 2003, *Seismic Performance of Highway Transportation Networks*, China-US Workshop on Protection of Urban Infrastructure and Public Buildings against Earthquakes and Manmade Disasters Beijing, China, 21-22 February 2003

Tokimatsu, A.M., and Seed, H.B., 1987, *Evaluation of Settlements in Sands Due to Earthquake Shaking*, Journal of the Geotechnical Division, American Society of Civil Engineers, Col. 113, No. 8, pp. 681-878.

USGS, 1997, San Francisco Bay Region Landslide Folio – Open-File Report 97-745, [http://wrgis.wr.usgs.gov/open-file/of97-745/].

USGS, 1999, *Earthquake Probabilities in the San Francisco Bay Region: 2000 to 2030, A Summary of Findings* – Open File Report 99-517, [http://geopubs.wr.usgs.gov/open-file/of99-517/].

USGS, 2000, Preliminary maps of quaternary deposits and liquefaction susceptibility, nine-county San Francisco Bay Region, California: a digital database – Open File Report 00-444, [http://geopubs.wr.usgs.gov/open-file/of00-444/].

USGS, 2003, Earthquake Probabilities in the San Francisco Bay Region: 2002–2031, Open File Report 03-214.

Wardrop, J., 1952, *Some Theoretical Aspects of Road Traffic Research*, Proceedings, Institution of Civil Engineers II, Volume 1, pp. 325–378.

Wells, D.L., and Coppersmith, K.J., 1994, *New empirical relationships among magnitude, rupture length, rupture width, rupture area, and surface displacement*, Bulletin of the Seismological Society of America, v. 84 #4, p. 974-1002.

Werner, S.D., Ostrom, D.K., and Taylor, C.E., 2002, *Planning unified lifeline risk/reliability platform for seismic risk decision making*, PEER Annual Reports, Pacific Earthquake Engineering Center, University of California, Berkeley.

Wieczorek, G.F., Wilson, R.C., and Harp., E.L., 1985, *Map Showing Slope Stability during Earthquakes in San Mateo County, CA*., USGS Map I-1257-E.

Wilson, R.C., and Keefer. D.K., 1985, *Predicting real limits of earthquake-induced landsliding*, Geological Survey, pp. 317-345.

Yanagihara, S., Takeuchi, M., and Ishihara, K., 1991, Dynamic Behavior of Embankment on Locally Compacted Sand Deposits, *Proceedings of the Fifth International Conference on Soil Dynamics and Earthquake Engineering* Computational Mechanics. Publication, Boston, and Elsevier Applied Science, pp. 365-376, New York 1991

Year 6 Annual Report, Pacific Earthquake Engineering Center, University of California, Berkeley.

Youd. T.L., and Perkins, D. M., 1978, *Mapping Liquefaction-induced Ground Failure Potential*, ASCE Journal of the Geotechnical Engineering Division, 104(4), pp. 433-446.

Appendix A: Liquefaction Computation

A method of estimating the maximum deformation due to liquefaction is presented in the HAZUS (1999) technical manual and is based on the approach of Youd and Perkins (1978). This method categorizes soils according to their susceptibility to liquefy and then defines the expected value of the permanent ground deformation due to lateral spreading and ground shaking. The susceptibility of each site to liquefy is expressed by its liquefaction susceptibility category.

However, it is not always the case that liquefaction occurs after an earthquake. The likelihood of experiencing liquefaction at a specific site is primarily influenced by the susceptibility of the soil to liquefaction, the amplitude and duration of the ground shaking, and depth of the groundwater. Therefore, the probability of liquefaction for a given susceptibility category is determined by the following relationship:

$$P[\,Liquefaction\,] = \frac{P[\,Liq \mid PGA = a\,]}{K_M K_W} P_{ml} \tag{A.1}$$

$$K_M = 0.0027M^3 - 0.0267M^2 - 0.2055M + 2.9188 \tag{A.1a}$$

$$K_W = 0.022 d_W + 0.93 \quad \text{(A.1b)}$$

where

P[Liq|PGA=a]	is the conditional probability for a given susceptibility category at a specified level of peak ground acceleration;
K_M	is the moment magnitude (M) correction factor computed in A.1a;
K_W	is the groundwater correction factor as a function of the water depth dW defined in A.1b; and
P_{ml}	is the proportion of map unit susceptible to liquefaction defined in Table A.1 below.

The conditional liquefaction probability relationships for all the liquefaction susceptibility categories are shown in Figure A.1, and the proportion of map unit susceptible to liquefaction is shown in Table A.1.

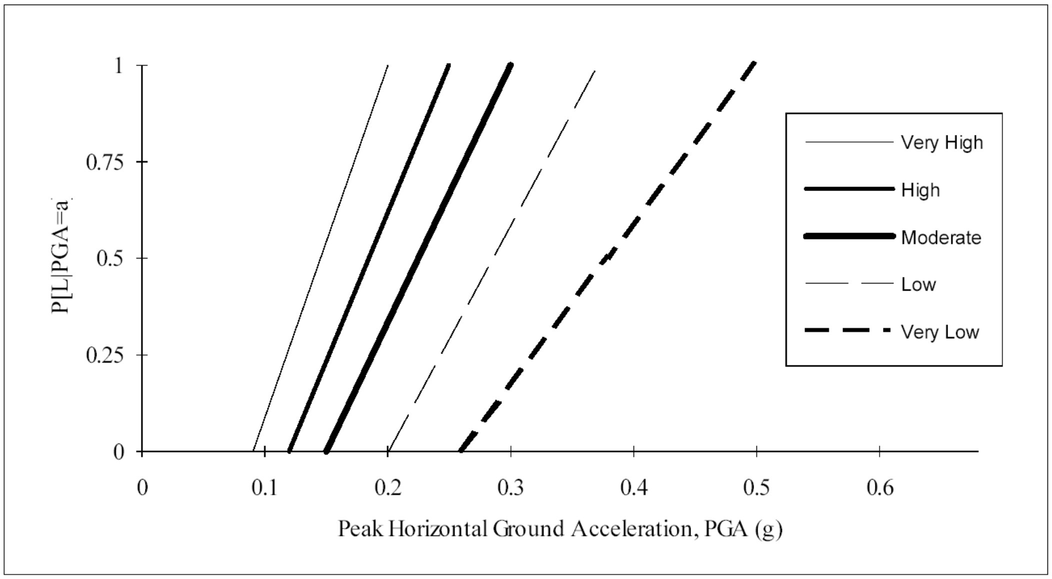

Fig. A.1 Conditional liquefaction probability relationships for liquefaction susceptibility categories (from Liao et al. 1988, HAZUS Technical Manual 1999).

Table A.1 Map unit susceptible to liquefaction (from HAZUS 1999).

Mapped Relative Susceptibility	Proportion of Map Unit
Very High	0.25
High	0.2
Moderate	0.1
Low	0.05
Very Low	0.02
None	0

After the calculation of the probability experiencing liquefaction at a site, the expected value of the permanent ground displacements due to lateral spreading is found. The relationship used is developed by combining the liquefaction severity index (LSI) relationship presented by Youd and Perkins (1987) with the ground motion attenuation relationship developed by Sadigh, et al. (1986).

The expected permanent ground displacement due to lateral spreading is then determined by the relationship:

$$E[PGD] = K_\Delta * E[PGD \mid PGA = a] \qquad \text{(A.2)}$$

$$K_\Delta = 0.0086M^3 - 0.0914M^2 + 0.4698M - 0.9835 \qquad \text{(A.2a)}$$

where

E[PGD/(PGA=a)] is the expected permanent ground displacement for a given susceptibility category under a specified level of normalized ground shaking. The normalization is made with the values corresponding to zero probability of liquefaction (PGA(t)). The expected value of the displacement is then defined in Figure A.1.

PGA(t) is the threshold value of the ground acceleration necessary to induce liquefaction (normalization value). It is defined in Table A.2.

K_Δ is the displacement correction factor as a function of the moment magnitude introduced by Seed and Idriss (1982). It is defined in equation A.2a.

Table A.2 Threshold ground acceleration corresponding to zero probability of liquefaction.

Susceptibility Category	PGA(t) in g
Very High	0.09
High	0.12
Moderate	0.15
Low	0.21
Very Low	0.26
None	N/A

The permanent ground deformation due to ground settlement associated with liquefaction is assumed to be related with the susceptibility category assigned to each location. This assumption is consistent with the work presented by Tokimatsu and Seed (1987) and Ishihara (1991) that indicate strong correlations between strain (settlement) and soil relative density (a measure of susceptibility). Based on these considerations, the ground settlement amplitudes are given in

Table A.3 for the portion of a soil deposit estimated to experience liquefaction at a given ground motion level.

Hence, the expected settlement at a location is the product of the probability to experience liquefaction for a given ground motion level and the characteristic settlement amplitude appropriate to the susceptibility category.

Table A.3 Ground settlement amplitudes for liquefaction susceptibility categories.

Relative Susceptibility	Settlement (inches)
Very High	12
High	6
Moderate	2
Low	1
Very Low	0
None	0

The combined effect of the two different causes of liquefaction described above, lateral spreading and ground settlement, is assumed to be the maximum of the individual PGD.

$$PGD_{Liq} = \max\{PGD_{LS}, PGD_{GS}\} \tag{A.3}$$

where

PGD_{LS} is the permanent ground deformation due to lateral spreading; and

PGD_{GS} is the permanent ground deformation due to ground settlement

In the last relationship the hypothesis is that the expected displacement due to lateral spreading for a normalized ground shaking cannot exceed 100 in.

Appendix B: Landslide Computation

The landslide hazard evaluation requires the characterization of the landslide susceptibility of the soil/geologic conditions at each site determined by the geologic group, the slope angle, and the critical acceleration. The landslide susceptibility geologic groups are shown in Table B.1 The categorization of the landslide susceptibility category at each bridge site is based on the work of Kiremidjian et al. (2003) for the Highway Demonstration Project.

Table B.1 Landslide susceptibility geologic groups (from HAZUS 1999).

Geologic Group		Slope Angle, degrees					
		0-10	10-15	15-20	20-30	30-40	>40
(a) DRY (groundwater below level of sliding)							
A	**Strongly Cemented Rocks (crystalline rocks and well-cemented sandstone, $c' = 300$ psf, $\phi' = 35^o$)**	None	None	I	II	IV	VI
B	**Weakly Cemented Rocks and Soils (sandy soils and poorly cemented sandstone, $c' = 0$, $\phi' = 35^o$)**	None	III	IV	V	VI	VII
C	**Argillaceous Rocks (shales, clayey soil, existing landslides, poorly compacted fills, $c' = 0$ $\phi' = 20^o$)**	V	VI	VII	IX	IX	IX
(b) WET (groundwater level at ground surface)							
A	**Strongly Cemented Rocks (crystalline rocks and well-cemented sandstone, $c' = 300$ psf, $\phi' = 35^o$)**	None	III	VI	VII	VIII	VIII
B	**Weakly Cemented Rocks and Soils (sandy soils and poorly cemented sandstone, $c' = 0$, $\phi' = 35^o$)**	V	VIII	IX	IX	IX	X
C	**Argillaceous Rocks (shales, clayey soil, existing landslides, poorly compacted fills, $c' = 0$ $\phi' = 20^o$)**	VII	IX	X	X	X	X

The critical acceleration for each susceptibility category is defined as a function of the critical acceleration with the help of Table B.2 Then using the relationship proposed by Wilson and Keefer (1985) as shown in Figure B.1 the susceptibility categories are assigned.

Table B.2 Critical accelerations for susceptibility categories (from HAZUS 1999).

Susceptibility Category	I	II	III	IV	V	VI	VII	VIII	IX	X
Critical Acceleration a_c (g)	0.6	0.5	0.4	0.35	0.3	0.25	0.2	0.15	0.1	0.05

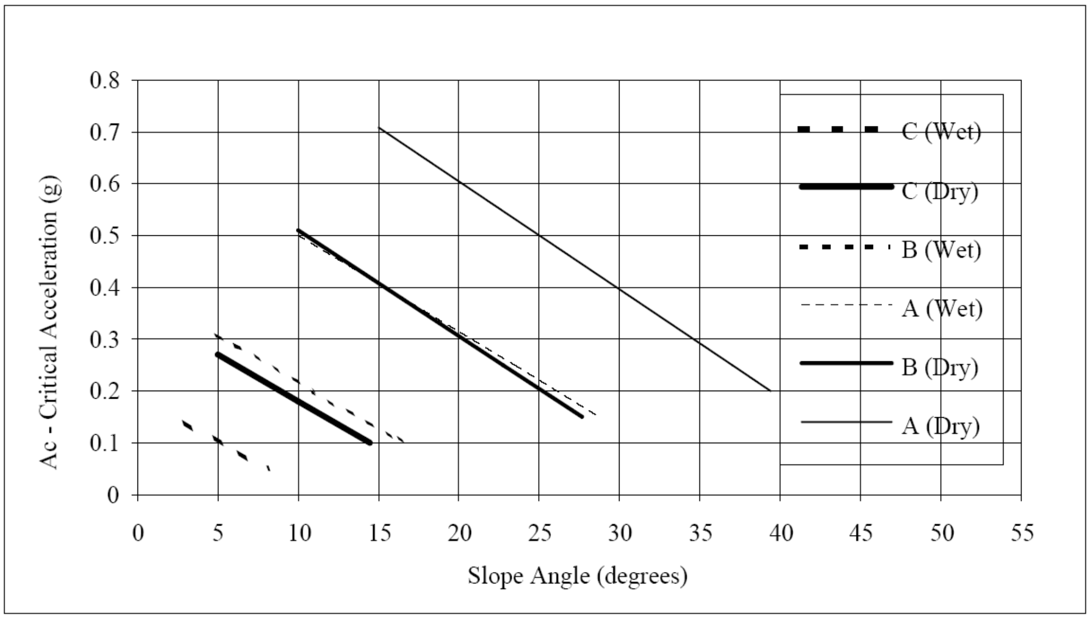

Fig. B.1 Critical acceleration as function of geologic group and slope angle (from Wilson and Keefer 1985).

The permanent ground displacements are then defined using the Equation B.1

$$E[PGD] = E[d \mid a_{is}] * a_{is} * n \tag{B.1}$$

$$n = 0.3419M^3 - 5.5214M^2 + 33.6154M - 70.7692 \tag{B.1a}$$

where

$E[d|a_{is}]$ is the expected displacement factor shown in Figure B.2. The produced equation is found after regression analysis with a second-order polynomial, based on the graph presented by Makdisi and Seed (1978).

a_{is} is the induced acceleration (in decimal fraction of g’s).

n is the number of cycles as a function of the magnitude of the moment magnitude (M) defined in Equation B.1a.

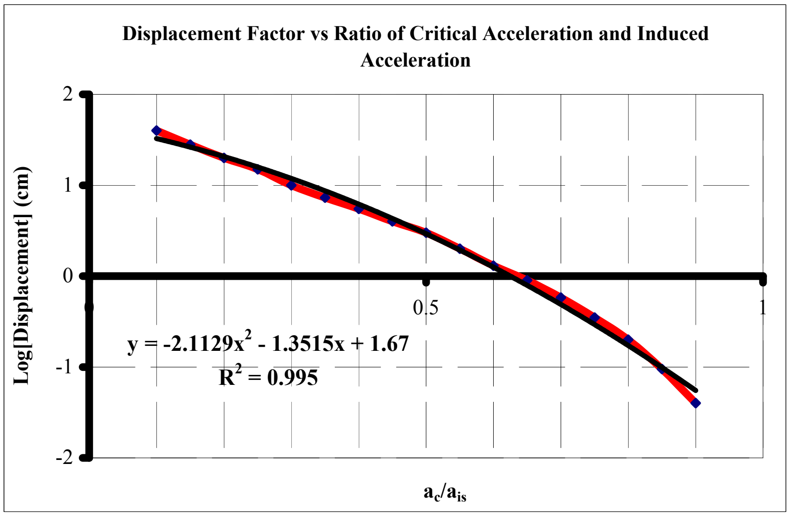

Fig. B.2 Relationship between displacement factor and ratio of critical acceleration and induced acceleration (from HAZUS 1999).

Because of the conservative nature of the Wilson and Keefer equation (1985), an assessment of the percentage of the landslide susceptibility category that is expected to fail is made. Wieczorek and others (1985) suggest values of probability for each susceptibility category, which are shown in Table B.3. The final value of the deformation due to landslide will be the product of the probability and the expected value.

Table B.3 Percentage of map area having landslide susceptible deposit (from HAZUS 1999).

Susceptibility Category	I	II	III	IV	V	VI	VII	VIII	IX	X
Map Area	0.00	0.01	0.01	0.03	0.05	0.08	0.10	0.20	0.25	0.30

Appendix C: Fragility Functions Computation

C.1 FRAGILITY FUNCTIONS FOR GROUND SHAKING

There are 28 primary bridge types for which all four damage states are identified and described. The median values of the acceleration for each damage state suggested by HAZUS (1999) are modified to take into account the characteristics of each bridge. The modification depends on the angle of skewness and the number of the spans of the bridge. The angle of skewness is defined as the angle between the centerline of the pier and a line normal to the roadway centerline. For the cases for which information regarding the angle of skewness are not available, it is assumed to be zero. The base bridge fragilities are modified by three parameters, K_{skew}, K_{shape}, and K_{3D}, respectively, accounting for skewness, shape, and three-dimensional effects. These empirical factors are computed after the following equations.

$$K_{skew} = \sqrt{\sin(90-a)} \tag{C.1}$$

where a is the skew angle

$$K_{shape} = 2.5 * S_a(1.0) / S_a(0.3) \tag{C.2}$$

where

Sa(1.0), Sa(0.3) is the spectral acceleration at the site for period equal to 1 and 0.3, respectively

$$K_{3D} = 1 + A/(N-B) \tag{C.3}$$

where A and B are parameters given in Table C.1 below.

Table C.1 Coefficients for evaluating K3D (from HAZUS 1999).

Equation	A	B	K_{3D}
EQ1	0.25	1	1 + 0.25 / (N – 1)
EQ2	0.33	0	1 + 0.33 / (N)
EQ3	0.33	1	1 + 0.33 / (N – 1)
EQ4	0.09	1	1 + 0.09 / (N – 1)
EQ5	0.05	0	1 + 0.05 / (N)
EQ6	0.20	1	1 + 0.20 / (N – 1)
EQ7	0.10	0	1 + 0.10 / (N)

Equation C.3 is used for K_{3D} defined by the category of the bridge as shown in Table C.1. For bridge class 28, the value of K_{3D} is not defined; thus, it is assumed to be 1. The modified medians are found according to the algorithm:

$$\begin{aligned}
&\text{New Median}_{\text{Slight}} = S_{\text{a,median,Slight}} * \text{Factor}_{\text{Slight}} \\
&\text{New Median}_{\text{Moderate}} = S_{\text{a,median,Moderate}} * K_{\text{skew}} * K_{3D} \\
&\text{New Median}_{\text{Extensive}} = S_{\text{a,median,Extensive}} * K_{\text{skew}} * K_{3D} \\
&\text{New Median}_{\text{Complete}} = S_{\text{a,median,Complete}} * K_{\text{skew}} * K_{3D}
\end{aligned} \qquad \text{(C.4)}$$

where

$\text{Factor}_{\text{Slight}} = 1$ if $I_{\text{shape}} = 0$ or

$\text{Factor}_{\text{Slight}} = \min(1, K_{\text{shape}})$ if $I_{\text{shape}} = 1$

The parameter I_{shape} is given by HAZUS for each bridge category. The standard deviation was taken $\beta = 0.6$ for all the cases.

C.2 FRAGILITY FUNCTIONS FOR GROUND DEFORMATION

Unlike the five damage states that can be observed in ground shaking, it is assumed that only damage states 1, 4, and 5 can be observed in ground failure. This constraint implies that the medians for damage states 2, 3, and 4 are equal. It practically means that damage states 2 and 3 never occur.

Similar to ground shaking, a modification procedure is followed to find the new medians for each bridge. It is made with the help of Table 3.4, where the modification parameters for all the categories are shown. For this modification, the assumption that if the angle of skewness is zero or infinite, then it is equal to one needed to be done, since it is not possible to have the median value of a lognormal distribution outside the interval (0,inf). The equations used for the modification are shown below.

$$\begin{aligned}
\text{New Median}_{\text{Slight}} &= S_{\text{d,median,Slight}} * f_1 \\
\text{New Median}_{\text{Moderate}} &= S_{\text{d,median,Moderate}} * f_1 \\
\text{New Median}_{\text{Extensive}} &= S_{\text{d,median,Extensive}} * f_1 \\
\text{New Median}_{\text{Complete}} &= S_{\text{d,median,Complete}} * f_2
\end{aligned} \tag{C.5}$$

The parameters *f1, f2* are defined in Table C.2 below. The standard deviation was taken $\beta = 0.2$ for all the cases.

Table C.2 Modifiers for PGD medians (from HAZUS 1999).

CLASS	f_1	f_2
HWB1	1	1
HWB2	1	1
HWB3	1	1
HWB4	1	1
HWB5	$0.5 * L / [N . W . \sin(\alpha)]$	$0.5 * L / [N . W . \sin(\alpha)]$
HWB6	$0.5 * L / [N . W . \sin(\alpha)]$	$0.5 * L / [N . W . \sin(\alpha)]$
HWB7	$0.5 * L / [N . W . \sin(\alpha)]$	$0.5 * L / [N . W . \sin(\alpha)]$
HWB8	1	$\sin(\alpha)$
HWB9	1	$\sin(\alpha)$
HWB10	1	$\sin(\alpha)$
HWB11	1	$\sin(\alpha)$
HWB12	$0.5 * L / [N . W . \sin(\alpha)]$	$0.5 * L / [N . W . \sin(\alpha)]$
HWB13	$0.5 * L / [N . W . \sin(\alpha)]$	$0.5 * L / [N . W . \sin(\alpha)]$
HWB14	$0.5 * L / [N . W . \sin(\alpha)]$	$0.5 * L / [N . W . \sin(\alpha)]$
HWB15	1	$\sin(\alpha)$
HWB16	1	$\sin(\alpha)$
HWB17	$0.5 * L / [N . W . \sin(\alpha)]$	$0.5 * L / [N . W . \sin(\alpha)]$
HWB18	$0.5 * L / [N . W . \sin(\alpha)]$	$0.5 * L / [N . W . \sin(\alpha)]$
HWB19	$0.5 * L / [N . W . \sin(\alpha)]$	$0.5 * L / [N . W . \sin(\alpha)]$
HWB20	1	$\sin(\alpha)$
HWB21	1	$\sin(\alpha)$
HWB22	$0.5 * L / [N . W . \sin(\alpha)]$	$0.5 * L / [N . W . \sin(\alpha)]$
HWB23	$0.5 * L / [N . W . \sin(\alpha)]$	$0.5 * L / [N . W . \sin(\alpha)]$
HWB24	$0.5 * L / [N . W . \sin(\alpha)]$	$0.5 * L / [N . W . \sin(\alpha)]$
HWB25	$0.5 * L / [N . W . \sin(\alpha)]$	$0.5 * L / [N . W . \sin(\alpha)]$
HWB26	1	$\sin(\alpha)$
HWB27	1	$\sin(\alpha)$
HWB28	1	1

Appendix D: Tables with Locations and Loss Estimates of Scenarios

Table D.1 Rupture locations of the scenarios of San Andreas fault.

Scenario	Case	Fault	Mw	Coordinate A		Coordinate B	
				Longitude	Latitude	Longitude	Latitude
1	1	San Andreas	6.75	-121.6300	36.8000	-121.8167	37.0014
2	2	San Andreas	6.75	-121.8059	36.9898	-121.9928	37.1913
3	3	San Andreas	6.75	-121.9822	37.1796	-122.1696	37.3811
4	4	San Andreas	6.75	-122.1590	37.3695	-122.3469	37.5709
5	5	San Andreas	6.75	-122.3362	37.5593	-122.5246	37.7607
6	6	San Andreas	6.75	-122.5139	37.7491	-122.7027	37.9505
7	7	San Andreas	6.75	-122.6921	37.9389	-122.8813	38.1404
8	8	San Andreas	6.75	-122.8706	38.1287	-123.0604	38.3302
9	9	San Andreas	6.75	-123.0497	38.3186	-123.2400	38.5200
10	1	San Andreas	7.00	-121.6300	36.8000	-121.9160	37.1084
11	2	San Andreas	7.00	-121.7936	36.9764	-122.0800	37.2849
12	3	San Andreas	7.00	-121.9576	37.1529	-122.2446	37.4613
13	4	San Andreas	7.00	-122.1220	37.3293	-122.4097	37.6378
14	5	San Andreas	7.00	-122.2868	37.5058	-122.5751	37.8142
15	6	San Andreas	7.00	-122.4519	37.6822	-122.7410	37.9907
16	7	San Andreas	7.00	-122.6175	37.8587	-122.9072	38.1671
17	8	San Andreas	7.00	-122.7834	38.0351	-123.0739	38.3436
18	9	San Andreas	7.00	-122.9498	38.2116	-123.2409	38.5200
19	1	San Andreas	7.25	-121.6300	36.8000	-122.0684	37.2722
20	2	San Andreas	7.25	-121.7955	36.9783	-122.2344	37.4505
21	3	San Andreas	7.25	-121.9613	37.1565	-122.4013	37.6287
22	4	San Andreas	7.25	-122.1276	37.3348	-122.5686	37.8070
23	5	San Andreas	7.25	-122.2942	37.5130	-122.7363	37.9852
24	6	San Andreas	7.25	-122.4613	37.6913	-122.9044	38.1635
25	7	San Andreas	7.25	-122.6287	37.8695	-123.0729	38.3417
26	8	San Andreas	7.25	-122.7966	38.0478	-123.2419	38.5200
27	1	San Andreas	7.50	-121.6300	36.8000	-122.3023	37.5230
28	2	San Andreas	7.50	-121.8154	36.9994	-122.4886	37.7224
29	3	San Andreas	7.50	-122.0013	37.1988	-122.6763	37.9218
30	4	San Andreas	7.50	-122.1877	37.3982	-122.8645	38.1212
31	5	San Andreas	7.50	-122.3746	37.5976	-123.0532	38.3206
32	6	San Andreas	7.50	-122.5620	37.7970	-123.2424	38.5200
33	1	San Andreas	7.75	-121.6300	36.8000	-122.6620	37.9070
34	2	San Andreas	7.75	-121.8205	37.0043	-122.8539	38.1114
35	3	San Andreas	7.75	-122.0115	37.2086	-123.0477	38.3157
36	4	San Andreas	7.75	-122.2030	37.4130	-123.2421	38.5200
37	1	San Andreas	8.00	-121.6300	36.8000	-123.2166	38.4950

Table D.2 Rupture locations of scenarios of Hayward fault.

Scenario	Case	Fault	Mw	Coordinate A		Coordinate B	
				Longitude	Latitude	Longitude	Latitude
38	1	Hayward	6.75	-121.8030	37.4500	-121.9948	37.6494
39	2	Hayward	6.75	-121.8740	37.5238	-122.0658	37.7232
40	3	Hayward	6.75	-121.9450	37.5976	-122.1371	37.7970
41	4	Hayward	6.75	-122.0161	37.6714	-122.2084	37.8708
42	5	Hayward	6.75	-122.0873	37.7452	-122.2798	37.9446
43	6	Hayward	6.75	-122.1586	37.8190	-122.3512	38.0184
44	7	Hayward	6.75	-122.2299	37.8928	-122.4227	38.0922
45	8	Hayward	6.75	-122.3013	37.9666	-122.4943	38.1660
46	1	Hayward	7.00	-121.8030	37.4500	-122.0968	37.7553
47	2	Hayward	7.00	-121.8821	37.5321	-122.1760	37.8374
48	3	Hayward	7.00	-121.9612	37.6143	-122.2555	37.9196
49	4	Hayward	7.00	-122.0404	37.6964	-122.3351	38.0017
50	5	Hayward	7.00	-122.1198	37.7786	-122.4147	38.0839
51	6	Hayward	7.00	-122.1992	37.8607	-122.4944	38.1660
52	1	Hayward	7.25	-121.8030	37.4500	-122.2533	37.9174
53	2	Hayward	7.25	-121.8828	37.5329	-122.3334	38.0003
54	3	Hayward	7.25	-121.9628	37.6157	-122.4138	38.0831
55	4	Hayward	7.25	-122.0428	37.6986	-122.4944	38.1660
56	1	Hayward	7.50	-121.8030	37.4500	-122.4936	38.1656

Table D.3 Loss estimates for San Andreas fault scenarios.

Scenario	Case	Structural Loss		Ground Shaking		Liquefaction		Landslide		Network	Total
		E(x)	σ_x	E(x)	σ_x	E(x)	σ_x	E(x)	σ_x	E(x)	E(x)
1	1	9.9	4.7	5.7	1.5	9.6	4.5	0.0	0.0	0.2	10.1
2	2	130.7	25.2	3.6	4.1	13.0	25.1	1.3	0.8	1.4	132.1
3	3	284.2	38.1	14.8	6.9	281.7	37.9	1.4	0.5	2.9	287.2
4	4	357.5	97.3	38.8	17.1	349.7	96.7	0.8	0.5	390.4	747.9
5	5	410.1	126.7	77.5	36.5	402.8	126.2	0.2	0.1	414.5	824.6
6	6	265.9	127.4	21.4	28.5	258.4	126.9	0.0	0.0	33.5	299.5
7	7	69.5	77.3	1.5	6.2	68.2	77.1	0.0	0.0	0.2	69.7
8	8	0.3	0.2	0.3	0.2	0.0	0.0	0.0	0.0	0.0	0.3
9	9	0.1	0.1	0.1	0.1	0.0	0.0	0.0	0.0	0.0	0.1
10	1	92.2	21.8	3.3	4.2	90.7	21.6	32.6	9.8	1.1	93.3
11	2	289.1	39.6	14.8	8.1	285.8	39.4	1.5	0.5	2.7	291.7
12	3	462.4	89.8	42.8	13.5	456.1	89.4	2.4	0.8	138.2	600.6
13	4	710.8	139.0	119.7	35.7	701.7	138.5	1.6	0.7	731.6	1,442.4
14	5	518.1	120.2	125.3	47.6	508.4	119.2	0.9	0.6	620.8	1,138.9
15	6	391.0	117.8	72.9	44.3	383.8	116.9	0.7	0.1	287.8	678.8
16	7	205.5	115.9	9.6	17.8	199.1	115.6	0.0	0.0	26.6	232.1
17	8	42.9	62.2	1.7	6.0	41.4	62.0	0.0	0.0	0.0	42.9
18	9	0.4	2.8	0.4	2.8	0.0	0.0	0.0	0.0	0.0	0.4
19	1	367.9	46.5	26.2	11.5	362.5	46.0	1.5	0.4	3.2	371.1
20	2	547.1	92.8	68.0	18.6	536.4	92.0	4.0	1.7	682.4	1,229.5
21	3	875.1	140.9	176.9	44.1	862.2	140.1	5.4	3.3	941.5	1,816.6
22	4	831.2	125.5	213.6	59.6	811.6	121.2	7.2	3.5	926.2	1,757.4
23	5	589.8	120.7	178.3	59.0	569.1	116.2	4.9	2.0	632.5	1,222.3
24	6	437.2	118.0	105.8	55.6	419.1	113.6	2.8	0.6	305.5	742.7
25	7	251.7	127.7	18.2	24.4	240.9	127.2	0.0	0.0	27.4	279.1
26	8	76.3	77.6	4.0	9.5	72.9	77.2	0.0	0.0	0.0	76.3
27	1	811.1	133.8	149.2	35.2	790.8	133.1	15.9	8.8	918.6	1,729.7
28	2	975.3	127.6	306.6	71.0	946.7	121.1	36.7	14.0	1,095.1	2,070.4
29	3	965.5	127.5	305.5	71.2	936.5	121.0	36.6	22.9	1,082.1	2,047.6
30	4	854.4	125.5	276.8	70.5	825.6	118.9	34.4	15.0	1,082.1	1,936.5
31	5	594.7	120.8	213.7	68.7	566.1	114.1	20.3	10.7	608.5	1,203.1
32	6	363.7	119.1	67.6	50.3	345.7	117.6	0.0	0.0	181.5	545.2
33	1	1,092.6	126.6	407.4	80.9	1,057.4	117.9	61.2	26.4	1,225.7	2,318.3
34	2	1,088.4	126.5	406.2	81.2	1,053.0	117.8	61.3	23.3	1,241.1	2,329.5
35	3	1,071.2	126.5	401.7	81.0	1,035.4	117.8	61.4	15.5	1,190.2	2,261.4
36	4	954.2	125.5	355.1	79.8	918.9	116.8	58.2	19.6	1,097.9	2,052.1
37	1	1,179.5	123.2	520.9	88.5	1,134.3	112.8	88.7	50.6	1,376.6	2,556.1

Table D.4 Loss estimates for Hayward fault scenarios.

Scenario	Case	Structural Loss		Ground Shaking		Liquefaction		Landslide		Network	Total
		E(x)	σ_x	E(x)	σ_x	E(x)	σ_x	E(x)	σ_x	E(x)	E(x)
38	1	364.5	73.1	16.5	9.2	361.2	72.8	0.0	0.0	461.1	825.6
39	2	388.5	88.1	23.6	11.9	384.6	87.9	0.0	0.0	494.1	882.7
40	3	457.8	95.5	35.5	17.2	453.3	95.2	0.0	0.0	510.9	968.7
41	4	485.8	104.8	50.1	21.4	480.6	104.4	0.0	0.0	563.0	1,048.8
42	5	472.2	104.7	47.8	21.3	467.8	104.3	0.0	0.0	530.3	1,002.6
43	6	405.1	103.5	44.6	21.1	400.7	103.1	0.0	0.0	316.0	721.1
44	7	337.0	102.4	32.8	19.4	332.9	102.0	0.0	0.0	214.7	551.6
45	8	224.4	89.6	13.6	13.2	221.1	89.2	0.0	0.0	116.9	341.3
46	1	653.3	103.2	57.6	20.7	646.6	102.7	0.0	0.0	989.4	1,642.7
47	2	708.0	123.2	83.6	27.5	699.9	122.8	0.1	0.0	1,070.4	1,778.3
48	3	644.3	124.0	84.4	28.4	634.8	123.6	0.2	0.1	1,032.6	1,677.0
49	4	598.5	123.2	83.4	28.4	589.6	122.8	0.2	0.1	980.2	1,578.7
50	5	547.6	122.8	73.0	27.9	539.9	122.4	0.2	0.1	639.6	1,187.2
51	6	462.2	121.5	63.5	27.4	454.6	121.1	0.1	0.0	307.7	769.9
52	1	930.4	138.8	148.5	37.8	916.6	138.2	1.0	0.4	1,966.7	2,897.1
53	2	877.6	138.6	143.5	37.2	863.7	138.0	1.2	0.7	2,045.8	2,923.4
54	3	752.8	135.9	131.7	36.7	738.7	135.3	1.2	0.3	1,948.6	2,701.5
55	4	673.2	134.5	124.8	36.5	658.6	133.8	1.2	0.7	1,848.3	2,521.6
56	1	1,013.6	139.5	221.1	47.5	993.3	138.5	9.7	3.4	2,129.5	3,143.1

PEER REPORTS

PEER reports are available from the National Information Service for Earthquake Engineering (NISEE). To order PEER reports, please contact the Pacific Earthquake Engineering Research Center, 1301 South 46th Street, Richmond, California 94804-4698. Tel.: (510) 665-3405; Fax: (510) 665-3420.

PEER 2008/02 *Treatment of Uncertainties in Seismic-Risk Analysis of Transportation Systems.* Evangelos Stergiou and Anne S. Kiremidjian. July 2008.

PEER 2007/11 *Bar Buckling in Reinforced Concrete Bridge Columns.* Wayne A. Brown, Dawn E. Lehman, and John F. Stanton. February 2008.

PEER 2007/10 *Computational Modeling of Progressive Collapse in Reinforced Concrete Frame Structures.* Mohamed M. Talaat and Khalid M. Mosalam. May 2008.

PEER 2007/09 *Integrated Probabilistic Performance-Based Evaluation of Benchmark Reinforced Concrete Bridges.* Kevin R. Mackie, John-Michael Wong, and Božidar Stojadinović. January 2008.

PEER 2007/08 *Assessing Seismic Collapse Safety of Modern Reinforced Concrete Moment-Frame Buildings.* Curt B. Haselton and Gregory G. Deierlein. February 2008.

PEER 2007/07 *Performance Modeling Strategies for Modern Reinforced Concrete Bridge Columns.* Michael P. Berry and Marc O. Eberhard. April 2008.

PEER 2007/06 *Development of Improved Procedures for Seismic Design of Buried and Partially Buried Structures.* Linda Al Atik and Nicholas Sitar. June 2007.

PEER 2007/05 *Uncertainty and Correlation in Seismic Risk Assessment of Transportation Systems.* Renee G. Lee and Anne S. Kiremidjian. July 2007.

PEER 2007/04 *Numerical Models for Analysis and Performance-Based Design of Shallow Foundations Subjected to Seismic Loading.* Sivapalan Gajan, Tara C. Hutchinson, Bruce L. Kutter, Prishati Raychowdhury, José A. Ugalde, and Jonathan P. Stewart. May 2008.

PEER 2007/03 *Beam-Column Element Model Calibrated for Predicting Flexural Response Leading to Global Collapse of RC Frame Buildings.* Curt B. Haselton, Abbie B. Liel, Sarah Taylor Lange, and Gregory g. Deierlein. May 2008.

PEER 2007/02 *Campbell-Bozorgnia NGA Ground Motion Relations for the Geometric Mean Horizontal Component of Peak and Spectral Ground Motion Parameters.* Kenneth W. Campbell and Yousef Bozorgnia. May 2007.

PEER 2007/01 *Boore-Atkinson NGA Ground Motion Relations for the Geometric Mean Horizontal Component of Peak and Spectral Ground Motion Parameters.* David M. Boore and Gail M. Atkinson. May. May 2007.

PEER 2006/12 *Societal Implications of Performance-Based Earthquake Engineering.* Peter J. May. May 2007.

PEER 2006/11 *Probabilistic Seismic Demand Analysis Using Advanced Ground Motion Intensity Measures, Attenuation Relationships, and Near-Fault Effects.* Polsak Tothong and C. Allin Cornell. March 2007.

PEER 2006/10 *Application of the PEER PBEE Methodology to the I-880 Viaduct.* Sashi Kunnath. February 2007.

PEER 2006/09 *Quantifying Economic Losses from Travel Forgone Following a Large Metropolitan Earthquake.* James Moore, Sungbin Cho, Yue Yue Fan, and Stuart Werner. November 2006.

PEER 2006/08 *Vector-Valued Ground Motion Intensity Measures for Probabilistic Seismic Demand Analysis*. Jack W. Baker and C. Allin Cornell. October 2006.

PEER 2006/07 *Analytical Modeling of Reinforced Concrete Walls for Predicting Flexural and Coupled–Shear-Flexural Responses.* Kutay Orakcal, Loenardo M. Massone, and John W. Wallace. October 2006.

PEER 2006/06 *Nonlinear Analysis of a Soil-Drilled Pier System under Static and Dynamic Axial Loading.* Gang Wang and Nicholas Sitar. November 2006.

PEER 2006/05 *Advanced Seismic Assessment Guidelines.* Paolo Bazzurro, C. Allin Cornell, Charles Menun, Maziar Motahari, and Nicolas Luco. September 2006.

PEER 2006/04 *Probabilistic Seismic Evaluation of Reinforced Concrete Structural Components and Systems.* Tae Hyung Lee and Khalid M. Mosalam. August 2006.

PEER 2006/03 *Performance of Lifelines Subjected to Lateral Spreading.* Scott A. Ashford and Teerawut Juirnarongrit. July 2006.

PEER 2006/02 *Pacific Earthquake Engineering Research Center Highway Demonstration Project.* Anne Kiremidjian, James Moore, Yue Yue Fan, Nesrin Basoz, Ozgur Yazali, and Meredith Williams. April 2006.

PEER 2006/01 *Bracing Berkeley. A Guide to Seismic Safety on the UC Berkeley Campus.* Mary C. Comerio, Stephen Tobriner, and Ariane Fehrenkamp. January 2006.

PEER 2005/16 *Seismic Response and Reliability of Electrical Substation Equipment and Systems.* Junho Song, Armen Der Kiureghian, and Jerome L. Sackman. April 2006.

PEER 2005/15 *CPT-Based Probabilistic Assessment of Seismic Soil Liquefaction Initiation.* R. E. S. Moss, R. B. Seed, R. E. Kayen, J. P. Stewart, and A. Der Kiureghian. April 2006.

PEER 2005/14 *Workshop on Modeling of Nonlinear Cyclic Load-Deformation Behavior of Shallow Foundations*. Bruce L. Kutter, Geoffrey Martin, Tara Hutchinson, Chad Harden, Sivapalan Gajan, and Justin Phalen. March 2006.

PEER 2005/13 *Stochastic Characterization and Decision Bases under Time-Dependent Aftershock Risk in Performance-Based Earthquake Engineering.* Gee Liek Yeo and C. Allin Cornell. July 2005.

PEER 2005/12 *PEER Testbed Study on a Laboratory Building: Exercising Seismic Performance Assessment.* Mary C. Comerio, editor. November 2005.

PEER 2005/11 *Van Nuys Hotel Building Testbed Report: Exercising Seismic Performance Assessment.* Helmut Krawinkler, editor. October 2005.

PEER 2005/10 *First NEES/E-Defense Workshop on Collapse Simulation of Reinforced Concrete Building Structures.* September 2005.

PEER 2005/09 *Test Applications of Advanced Seismic Assessment Guidelines.* Joe Maffei, Karl Telleen, Danya Mohr, William Holmes, and Yuki Nakayama. August 2006.

PEER 2005/08 *Damage Accumulation in Lightly Confined Reinforced Concrete Bridge Columns.* R. Tyler Ranf, Jared M. Nelson, Zach Price, Marc O. Eberhard, and John F. Stanton. April 2006.

PEER 2005/07 *Experimental and Analytical Studies on the Seismic Response of Freestanding and Anchored Laboratory Equipment.* Dimitrios Konstantinidis and Nicos Makris. January 2005.

PEER 2005/06 *Global Collapse of Frame Structures under Seismic Excitations*. Luis F. Ibarra and Helmut Krawinkler. September 2005.

PEER 2005//05 *Performance Characterization of Bench- and Shelf-Mounted Equipment.* Samit Ray Chaudhuri and Tara C. Hutchinson. May 2006.

PEER 2005/04 *Numerical Modeling of the Nonlinear Cyclic Response of Shallow Foundations.* Chad Harden, Tara Hutchinson, Geoffrey R. Martin, and Bruce L. Kutter. August 2005.

PEER 2005/03 *A Taxonomy of Building Components for Performance-Based Earthquake Engineering.* Keith A. Porter. September 2005.

PEER 2005/02 *Fragility Basis for California Highway Overpass Bridge Seismic Decision Making*. Kevin R. Mackie and Božidar Stojadinović. June 2005.

PEER 2005/01 *Empirical Characterization of Site Conditions on Strong Ground Motion.* Jonathan P. Stewart, Yoojoong Choi, and Robert W. Graves. June 2005.

PEER 2004/09 *Electrical Substation Equipment Interaction: Experimental Rigid Conductor Studies.* Christopher Stearns and André Filiatrault. February 2005.

PEER 2004/08 *Seismic Qualification and Fragility Testing of Line Break 550-kV Disconnect Switches.* Shakhzod M. Takhirov, Gregory L. Fenves, and Eric Fujisaki. January 2005.

PEER 2004/07 *Ground Motions for Earthquake Simulator Qualification of Electrical Substation Equipment.* Shakhzod M. Takhirov, Gregory L. Fenves, Eric Fujisaki, and Don Clyde. January 2005.

PEER 2004/06 *Performance-Based Regulation and Regulatory Regimes.* Peter J. May and Chris Koski. September 2004.

PEER 2004/05 *Performance-Based Seismic Design Concepts and Implementation: Proceedings of an International Workshop.* Peter Fajfar and Helmut Krawinkler, editors. September 2004.

PEER 2004/04 *Seismic Performance of an Instrumented Tilt-up Wall Building.* James C. Anderson and Vitelmo V. Bertero. July 2004.

PEER 2004/03 *Evaluation and Application of Concrete Tilt-up Assessment Methodologies.* Timothy Graf and James O. Malley. October 2004.

PEER 2004/02 *Analytical Investigations of New Methods for Reducing Residual Displacements of Reinforced Concrete Bridge Columns.* Junichi Sakai and Stephen A. Mahin. August 2004.

PEER 2004/01 *Seismic Performance of Masonry Buildings and Design Implications.* Kerri Anne Taeko Tokoro, James C. Anderson, and Vitelmo V. Bertero. February 2004.

PEER 2003/18 *Performance Models for Flexural Damage in Reinforced Concrete Columns.* Michael Berry and Marc Eberhard. August 2003.

PEER 2003/17 *Predicting Earthquake Damage in Older Reinforced Concrete Beam-Column Joints.* Catherine Pagni and Laura Lowes. October 2004.

PEER 2003/16 *Seismic Demands for Performance-Based Design of Bridges.* Kevin Mackie and Božidar Stojadinović. August 2003.

PEER 2003/15 *Seismic Demands for Nondeteriorating Frame Structures and Their Dependence on Ground Motions.* Ricardo Antonio Medina and Helmut Krawinkler. May 2004.

PEER 2003/14 *Finite Element Reliability and Sensitivity Methods for Performance-Based Earthquake Engineering*. Terje Haukaas and Armen Der Kiureghian. April 2004.

PEER 2003/13 *Effects of Connection Hysteretic Degradation on the Seismic Behavior of Steel Moment-Resisting Frames.* Janise E. Rodgers and Stephen A. Mahin. March 2004.

PEER 2003/12 *Implementation Manual for the Seismic Protection of Laboratory Contents: Format and Case Studies.* William T. Holmes and Mary C. Comerio. October 2003.

PEER 2003/11 *Fifth U.S.-Japan Workshop on Performance-Based Earthquake Engineering Methodology for Reinforced Concrete Building Structures.* February 2004.

PEER 2003/10 *A Beam-Column Joint Model for Simulating the Earthquake Response of Reinforced Concrete Frames.* Laura N. Lowes, Nilanjan Mitra, and Arash Altoontash. February 2004.

PEER 2003/09 *Sequencing Repairs after an Earthquake: An Economic Approach.* Marco Casari and Simon J. Wilkie. April 2004.

PEER 2003/08 *A Technical Framework for Probability-Based Demand and Capacity Factor Design (DCFD) Seismic Formats*. Fatemeh Jalayer and C. Allin Cornell. November 2003.

PEER 2003/07 *Uncertainty Specification and Propagation for Loss Estimation Using FOSM Methods.* Jack W. Baker and C. Allin Cornell. September 2003.

PEER 2003/06 *Performance of Circular Reinforced Concrete Bridge Columns under Bidirectional Earthquake Loading*. Mahmoud M. Hachem, Stephen A. Mahin, and Jack P. Moehle. February 2003.

PEER 2003/05 *Response Assessment for Building-Specific Loss Estimation.* Eduardo Miranda and Shahram Taghavi. September 2003.

PEER 2003/04 *Experimental Assessment of Columns with Short Lap Splices Subjected to Cyclic Loads*. Murat Melek, John W. Wallace, and Joel Conte. April 2003.

PEER 2003/03 *Probabilistic Response Assessment for Building-Specific Loss Estimation.* Eduardo Miranda and Hesameddin Aslani. September 2003.

PEER 2003/02 *Software Framework for Collaborative Development of Nonlinear Dynamic Analysis Program.* Jun Peng and Kincho H. Law. September 2003.

PEER 2003/01 *Shake Table Tests and Analytical Studies on the Gravity Load Collapse of Reinforced Concrete Frames.* Kenneth John Elwood and Jack P. Moehle. November 2003.

PEER 2002/24 *Performance of Beam to Column Bridge Joints Subjected to a Large Velocity Pulse.* Natalie Gibson, André Filiatrault, and Scott A. Ashford. April 2002.

PEER 2002/23 *Effects of Large Velocity Pulses on Reinforced Concrete Bridge Columns.* Greg L. Orozco and Scott A. Ashford. April 2002.

PEER 2002/22 *Characterization of Large Velocity Pulses for Laboratory Testing.* Kenneth E. Cox and Scott A. Ashford. April 2002.

PEER 2002/21 *Fourth U.S.-Japan Workshop on Performance-Based Earthquake Engineering Methodology for Reinforced Concrete Building Structures*. December 2002.

PEER 2002/20 *Barriers to Adoption and Implementation of PBEE Innovations.* Peter J. May. August 2002.

PEER 2002/19 *Economic-Engineered Integrated Models for Earthquakes: Socioeconomic Impacts.* Peter Gordon, James E. Moore II, and Harry W. Richardson. July 2002.

PEER 2002/18 *Assessment of Reinforced Concrete Building Exterior Joints with Substandard Details.* Chris P. Pantelides, Jon Hansen, Justin Nadauld, and Lawrence D. Reaveley. May 2002.

PEER 2002/17 *Structural Characterization and Seismic Response Analysis of a Highway Overcrossing Equipped with Elastomeric Bearings and Fluid Dampers: A Case Study.* Nicos Makris and Jian Zhang. November 2002.

PEER 2002/16 *Estimation of Uncertainty in Geotechnical Properties for Performance-Based Earthquake Engineering.* Allen L. Jones, Steven L. Kramer, and Pedro Arduino. December 2002.

PEER 2002/15 *Seismic Behavior of Bridge Columns Subjected to Various Loading Patterns.* Asadollah Esmaeily-Gh. and Yan Xiao. December 2002.

PEER 2002/14 *Inelastic Seismic Response of Extended Pile Shaft Supported Bridge Structures.* T.C. Hutchinson, R.W. Boulanger, Y.H. Chai, and I.M. Idriss. December 2002.

PEER 2002/13 *Probabilistic Models and Fragility Estimates for Bridge Components and Systems.* Paolo Gardoni, Armen Der Kiureghian, and Khalid M. Mosalam. June 2002.

PEER 2002/12 *Effects of Fault Dip and Slip Rake on Near-Source Ground Motions: Why Chi-Chi Was a Relatively Mild M7.6 Earthquake.* Brad T. Aagaard, John F. Hall, and Thomas H. Heaton. December 2002.

PEER 2002/11 *Analytical and Experimental Study of Fiber-Reinforced Strip Isolators*. James M. Kelly and Shakhzod M. Takhirov. September 2002.

PEER 2002/10 *Centrifuge Modeling of Settlement and Lateral Spreading with Comparisons to Numerical Analyses***.** Sivapalan Gajan and Bruce L. Kutter. January 2003.

PEER 2002/09 *Documentation and Analysis of Field Case Histories of Seismic Compression during the 1994 Northridge, California, Earthquake.* Jonathan P. Stewart, Patrick M. Smith, Daniel H. Whang, and Jonathan D. Bray. October 2002.

PEER 2002/08 *Component Testing, Stability Analysis and Characterization of Buckling-Restrained Unbonded Braces™*. Cameron Black, Nicos Makris, and Ian Aiken. September 2002.

PEER 2002/07 *Seismic Performance of Pile-Wharf Connections.* Charles W. Roeder, Robert Graff, Jennifer Soderstrom, and Jun Han Yoo. December 2001.

PEER 2002/06 *The Use of Benefit-Cost Analysis for Evaluation of Performance-Based Earthquake Engineering Decisions*. Richard O. Zerbe and Anthony Falit-Baiamonte. September 2001.

PEER 2002/05 *Guidelines, Specifications, and Seismic Performance Characterization of Nonstructural Building Components and Equipment*. André Filiatrault, Constantin Christopoulos, and Christopher Stearns. September 2001.

PEER 2002/04 *Consortium of Organizations for Strong-Motion Observation Systems and the Pacific Earthquake Engineering Research Center Lifelines Program: Invited Workshop on Archiving and Web Dissemination of Geotechnical Data, 4–5 October 2001*. September 2002.

PEER 2002/03 *Investigation of Sensitivity of Building Loss Estimates to Major Uncertain Variables for the Van Nuys Testbed.* Keith A. Porter, James L. Beck, and Rustem V. Shaikhutdinov. August 2002.

PEER 2002/02 *The Third U.S.-Japan Workshop on Performance-Based Earthquake Engineering Methodology for Reinforced Concrete Building Structures*. July 2002.

PEER 2002/01 *Nonstructural Loss Estimation: The UC Berkeley Case Study.* Mary C. Comerio and John C. Stallmeyer. December 2001.

PEER 2001/16 *Statistics of SDF-System Estimate of Roof Displacement for Pushover Analysis of Buildings.* Anil K. Chopra, Rakesh K. Goel, and Chatpan Chintanapakdee. December 2001.

PEER 2001/15 *Damage to Bridges during the 2001 Nisqually Earthquake.* R. Tyler Ranf, Marc O. Eberhard, and Michael P. Berry. November 2001.

PEER 2001/14 *Rocking Response of Equipment Anchored to a Base Foundation.* Nicos Makris and Cameron J. Black. September 2001.

PEER 2001/13 *Modeling Soil Liquefaction Hazards for Performance-Based Earthquake Engineering.* Steven L. Kramer and Ahmed-W. Elgamal. February 2001.

PEER 2001/12 *Development of Geotechnical Capabilities in OpenSees.* Boris Jeremi . September 2001.

PEER 2001/11 *Analytical and Experimental Study of Fiber-Reinforced Elastomeric Isolators*. James M. Kelly and Shakhzod M. Takhirov. September 2001.

PEER 2001/10 *Amplification Factors for Spectral Acceleration in Active Regions.* Jonathan P. Stewart, Andrew H. Liu, Yoojoong Choi, and Mehmet B. Baturay. December 2001.

PEER 2001/09 *Ground Motion Evaluation Procedures for Performance-Based Design.* Jonathan P. Stewart, Shyh-Jeng Chiou, Jonathan D. Bray, Robert W. Graves, Paul G. Somerville, and Norman A. Abrahamson. September 2001.

PEER 2001/08 *Experimental and Computational Evaluation of Reinforced Concrete Bridge Beam-Column Connections for Seismic Performance*. Clay J. Naito, Jack P. Moehle, and Khalid M. Mosalam. November 2001.

PEER 2001/07 *The Rocking Spectrum and the Shortcomings of Design Guidelines.* Nicos Makris and Dimitrios Konstantinidis. August 2001.

PEER 2001/06 *Development of an Electrical Substation Equipment Performance Database for Evaluation of Equipment Fragilities.* Thalia Agnanos. April 1999.

PEER 2001/05 *Stiffness Analysis of Fiber-Reinforced Elastomeric Isolators.* Hsiang-Chuan Tsai and James M. Kelly. May 2001.

PEER 2001/04 *Organizational and Societal Considerations for Performance-Based Earthquake Engineering.* Peter J. May. April 2001.

PEER 2001/03 *A Modal Pushover Analysis Procedure to Estimate Seismic Demands for Buildings: Theory and Preliminary Evaluation.* Anil K. Chopra and Rakesh K. Goel. January 2001.

PEER 2001/02 *Seismic Response Analysis of Highway Overcrossings Including Soil-Structure Interaction.* Jian Zhang and Nicos Makris. March 2001.

PEER 2001/01 *Experimental Study of Large Seismic Steel Beam-to-Column Connections.* Egor P. Popov and Shakhzod M. Takhirov. November 2000.

PEER 2000/10 *The Second U.S.-Japan Workshop on Performance-Based Earthquake Engineering Methodology for Reinforced Concrete Building Structures.* March 2000.

PEER 2000/09 *Structural Engineering Reconnaissance of the August 17, 1999 Earthquake: Kocaeli (Izmit), Turkey.* Halil Sezen, Kenneth J. Elwood, Andrew S. Whittaker, Khalid Mosalam, John J. Wallace, and John F. Stanton. December 2000.

PEER 2000/08 *Behavior of Reinforced Concrete Bridge Columns Having Varying Aspect Ratios and Varying Lengths of Confinement.* Anthony J. Calderone, Dawn E. Lehman, and Jack P. Moehle. January 2001.

PEER 2000/07 *Cover-Plate and Flange-Plate Reinforced Steel Moment-Resisting Connections.* Taejin Kim, Andrew S. Whittaker, Amir S. Gilani, Vitelmo V. Bertero, and Shakhzod M. Takhirov. September 2000.

PEER 2000/06 *Seismic Evaluation and Analysis of 230-kV Disconnect Switches.* Amir S. J. Gilani, Andrew S. Whittaker, Gregory L. Fenves, Chun-Hao Chen, Henry Ho, and Eric Fujisaki. July 2000.

PEER 2000/05 *Performance-Based Evaluation of Exterior Reinforced Concrete Building Joints for Seismic Excitation.* Chandra Clyde, Chris P. Pantelides, and Lawrence D. Reaveley. July 2000.

PEER 2000/04 *An Evaluation of Seismic Energy Demand: An Attenuation Approach.* Chung-Che Chou and Chia-Ming Uang. July 1999.

PEER 2000/03 *Framing Earthquake Retrofitting Decisions: The Case of Hillside Homes in Los Angeles.* Detlof von Winterfeldt, Nels Roselund, and Alicia Kitsuse. March 2000.

PEER 2000/02 *U.S.-Japan Workshop on the Effects of Near-Field Earthquake Shaking.* Andrew Whittaker, ed. July 2000.

PEER 2000/01 *Further Studies on Seismic Interaction in Interconnected Electrical Substation Equipment.* Armen Der Kiureghian, Kee-Jeung Hong, and Jerome L. Sackman. November 1999.

PEER 1999/14 *Seismic Evaluation and Retrofit of 230-kV Porcelain Transformer Bushings*. Amir S. Gilani, Andrew S. Whittaker, Gregory L. Fenves, and Eric Fujisaki. December 1999.

PEER 1999/13 *Building Vulnerability Studies: Modeling and Evaluation of Tilt-up and Steel Reinforced Concrete Buildings.* John W. Wallace, Jonathan P. Stewart, and Andrew S. Whittaker, editors. December 1999.

PEER 1999/12 *Rehabilitation of Nonductile RC Frame Building Using Encasement Plates and Energy-Dissipating Devices.* Mehrdad Sasani, Vitelmo V. Bertero, James C. Anderson. December 1999.

PEER 1999/11 *Performance Evaluation Database for Concrete Bridge Components and Systems under Simulated Seismic Loads.* Yael D. Hose and Frieder Seible. November 1999.

PEER 1999/10 *U.S.-Japan Workshop on Performance-Based Earthquake Engineering Methodology for Reinforced Concrete Building Structures.* December 1999.

PEER 1999/09 *Performance Improvement of Long Period Building Structures Subjected to Severe Pulse-Type Ground Motions*. James C. Anderson, Vitelmo V. Bertero, and Raul Bertero. October 1999.

PEER 1999/08 *Envelopes for Seismic Response Vectors.* Charles Menun and Armen Der Kiureghian. July 1999.

PEER 1999/07 *Documentation of Strengths and Weaknesses of Current Computer Analysis Methods for Seismic Performance of Reinforced Concrete Members.* William F. Cofer. November 1999.

PEER 1999/06 *Rocking Response and Overturning of Anchored Equipment under Seismic Excitations.* Nicos Makris and Jian Zhang. November 1999.

PEER 1999/05 *Seismic Evaluation of 550 kV Porcelain Transformer Bushings.* Amir S. Gilani, Andrew S. Whittaker, Gregory L. Fenves, and Eric Fujisaki. October 1999.

PEER 1999/04 *Adoption and Enforcement of Earthquake Risk-Reduction Measures.* Peter J. May, Raymond J. Burby, T. Jens Feeley, and Robert Wood.

PEER 1999/03 *Task 3 Characterization of Site Response General Site Categories*. Adrian Rodriguez-Marek, Jonathan D. Bray, and Norman Abrahamson. February 1999.

PEER 1999/02 *Capacity-Demand-Diagram Methods for Estimating Seismic Deformation of Inelastic Structures: SDF Systems*. Anil K. Chopra and Rakesh Goel. April 1999.

PEER 1999/01 *Interaction in Interconnected Electrical Substation Equipment Subjected to Earthquake Ground Motions.* Armen Der Kiureghian, Jerome L. Sackman, and Kee-Jeung Hong. February 1999.

PEER 1998/08 *Behavior and Failure Analysis of a Multiple-Frame Highway Bridge in the 1994 Northridge Earthquake.* Gregory L. Fenves and Michael Ellery. December 1998.

PEER 1998/07 *Empirical Evaluation of Inertial Soil-Structure Interaction Effects.* Jonathan P. Stewart, Raymond B. Seed, and Gregory L. Fenves. November 1998.

PEER 1998/06 *Effect of Damping Mechanisms on the Response of Seismic Isolated Structures.* Nicos Makris and Shih-Po Chang. November 1998.

PEER 1998/05 *Rocking Response and Overturning of Equipment under Horizontal Pulse-Type Motions.* Nicos Makris and Yiannis Roussos. October 1998.

PEER 1998/04 *Pacific Earthquake Engineering Research Invitational Workshop Proceedings, May 14–15, 1998: Defining the Links between Planning, Policy Analysis, Economics and Earthquake Engineering.* Mary Comerio and Peter Gordon. September 1998.

PEER 1998/03 *Repair/Upgrade Procedures for Welded Beam to Column Connections.* James C. Anderson and Xiaojing Duan. May 1998.

PEER 1998/02 *Seismic Evaluation of 196 kV Porcelain Transformer Bushings.* Amir S. Gilani, Juan W. Chavez, Gregory L. Fenves, and Andrew S. Whittaker. May 1998.

PEER 1998/01 *Seismic Performance of Well-Confined Concrete Bridge Columns.* Dawn E. Lehman and Jack P. Moehle. December 2000.

ONLINE REPORTS

The following PEER reports are available by Internet only at http://peer.berkeley.edu/publications/peer_reports.html

PEER 2007/101 *Generalized Hybrid Simulation Framework for Structural Systems Subjected to Seismic Loading.* Tarek Elkhoraibi and Khalid M. Mosalam. July 2007.

PEER 2007/100 *Seismic Evaluation of Reinforced Concrete Buildings Including Effects of Masonry Infill Walls.* Alidad Hashemi and Khalid M. Mosalam. July 2007.